NTIA Report 98-355

Man-Made Noise in the 136 to 138-MHz VHF Meteorological Satellite Band

Robert J. Achatz
Yeh Lo
Peter B. Papazian
Roger A. Dalke
George A. Hufford

U.S. DEPARTMENT OF COMMERCE
William M. Daley, Secretary

Larry Irving, Assistant Secretary
for Communications and Information

September 1998

This Page Intentionally Left Blank

This Page Intentionally Left Blank

CONTENTS

Page

This Page Intentionally Left Blank

This Page Intentionally Left Blank

FIGURES

This Page Intentionally Left Blank

This Page Intentionally Left Blank

TABLES

This Page Intentionally Left Blank

This Page Intentionally Left Blank

This Page Intentionally Left Blank

This Page Intentionally Left Blank

MAN-MADE NOISE IN THE 136 to 138-MHz VHF METEOROLOGICAL SATELLITE BAND

[1]Robert Achatz, Yeh Lo, Peter Papazian, Roger Dalke, George Hufford

Satellite radio system performance in the 136 to 138-MHz VHF meteorological satellite band is compromised by man-made noise external to the receiver. Methods used for predicting man-made noise power in this band are based on measurements conducted in the 1970's. These methods may be inaccurate due to technological advances such as quieter automotive ignition systems and the proliferation of consumer electronic devices such as the personal computer. This report describes noise power measurements the Institute for Telecommunication Sciences performed in the 136 to 138-MHz VHF meteorological satellite band. Statistics of average noise power were compared to those of measurements conducted in the 1970's. The noise power measurements were also used to model instantaneous noise power for simulation of radio links.

Key words: radio channel, man-made noise, impulsive noise, non-Gaussian noise, meteorological satellite, satellite communications, simulation of communication systems, noise measurement, noise modeling.

1. INTRODUCTION

In 1974, Spaulding and Disney [1] presented results that summarized many years of measurements of radio noise - both natural and man-made. From these results they devised methods for estimating the noise power statistics that are important in the design of radio systems. These methods are described in the CCIR Reports [2,3] and have been widely used by industry. Figure 1.1, taken from these reports, presents the median antenna noise figure (a measure of the environment's average noise power) from 0.1 to 1000.0 MHz. The graph shows that contributions in the 136 to 138-MHz VHF meteorological satellite band by atmospheric noise (distant lightning) or galactic sources are minimal, and that man-made noise in business, residential, or rural environments might be significant.

In recent reports, Spaulding [4,5] has warned that the CCIR methods - at least when referring to man-made noise - may have been made inaccurate by technological advances. For example, newer automobile ignition systems radiate less noise, but personal computers capable of producing considerable noise have become ubiquitous in business and residential environments. Thus, measurement and modeling of man-made noise is timely for the design of VHF meteorological satellite radio systems [6,7].

We began our noise power measurement and modeling campaign by building a noise power measurement receiver and writing computer software that digitized and stored noise power samples

[1]The authors are with the Institute for Telecommunication Sciences, National Telecommunications and Information Administration, U.S. Department of Commerce, Boulder, CO 80303-3328

for later analysis. The receiver and computer were installed in a van that was driven to rural, residential, and business environments for data collection. We also attempted to isolate noise power generated by automobiles, the electrical distribution network, and electronic devices.

The data, stored in histograms representing two minutes of noise power samples, were analyzed in two distinct ways. First, the statistical behavior of each histogram's average power was analyzed for rural, residential, and business environments. Second, the first-order statistics of instantaneous noise power within a histogram were studied. Algorithms capable of generating noise with similar first-order statistics were then created for simulation of radio links.

This section continues with a review of the terminology used to describe radio noise. Section 2 describes the noise measurement equipment. Section 3 gives an overview of the measurements taken. Section 4 summarizes the average noise power in rural, residential, and business environments. Section 5 analyzes first-order statistics of instantaneous noise power and presents a discrete noise model for simulation of radio links. Section 6 summarizes our findings.

1.1. Background and Terminology

1.1.1 Noise Voltage Representations

A noise voltage is a random function of time whose behavior only can be described statistically. The time-varying noise voltage, *v(t)*, is represented as a *passband* signal centered about a carrier frequency, f_c,

$$v(t) = Re\left\{\hat{v}(t)e^{j2\pi f_c t}\right\}, \tag{1.1}$$

where *Re*{} denotes the real part and $\hat{v}(t)$ is the noise voltage *complex baseband* signal centered about 0 Hz that can be represented in Cartesian or polar form as follows:

$$\hat{v}(t) = x(t) + j\,y(t) = \sqrt{x(t)^2 + y(t)^2}\; e^{\,j \arctan\left(\frac{y(t)}{x(t)}\right)}. \tag{1.2}$$

where *x(t)* and *y(t)* are the baseband signal real and imaginary components, respectively. Both *v(t)* and $\hat{v}(t)$ are random processes defined by one or more random variables. For example, if *v(t)* is *white Gaussian noise* it is represented by a *Gaussian distributed* random variable whose mean is zero and *power spectral density* (PSD) is flat. The baseband real and imaginary components of white Gaussian noise are *independent and identically distributed* Gaussian random variables with zero means and flat PSD's. The baseband amplitude and phase of white Gaussian noise are independent but not identically distributed random variables. The amplitude random variable is *Rayleigh distributed* while the phase random variable is *uniformly distributed*.

1.1.2 Instantaneous Noise Power

We define the *instantaneous noise power* as

$$w = |\hat{v}(t)|^2 \ . \tag{1.3}$$

In this report the instantaneous noise power is normalized by the average noise power due to black-body radiation and thermal noise that is present in all radio systems. This average noise power is kT_0b where $k = 1.38\text{x}10^{-23}$ W/Hz/K is Boltzman's constant, $T_0 = 288$K is the absolute temperature, and b is the receiver *noise equivalent bandwidth*.

1.1.3 Statistics of Instantaneous Noise Power

The *cumulative distribution function (CDF)* of instantaneous noise power describes the probability that the noise power will not exceed a value

$$P(W_{RV} \leq w) = \int_0^w p(x)dx \ , \tag{1.4}$$

where W_{RV} is the noise power random variable, w is the noise power independent variable, and $p(w)$ is the *probability density function (PDF)* of the noise power random variable. Radio engineers are concerned with the probability that the noise power will exceed a value. This probability is expressed as

$$A(w) = P(W_{RV} > w) = \int_w^\infty p(x)dx \tag{1.5}$$

and is customarily referred to as the *amplitude probability distribution* function (APD).

For white Gaussian noise, the amplitude PDF, expressed in w, is

$$P(w) = \frac{1}{w_0} e^{-\frac{w}{w_0}} \ , \tag{1.6}$$

the amplitude CDF, expressed in w, is

$$P(W_{RV} \leq w) = 1 - e^{-\frac{w}{w_0}} \ , \tag{1.7}$$

and the APD, expressed in w, is

$$A(w) = P(W_{RV} > w) = e^{-\frac{w}{w_0}} . \tag{1.8}$$

In this report APD's are plotted on a *Rayleigh probability graph* whose axes represent the amplitude in dB above kT_0b and the percent of time the amplitude is exceeded. On a Rayleigh probability graph, noise with a Rayleigh amplitude distribution forms a straight line with slope -1/2 whose mean lies on the 37.0 percentile, median lies on the 50.0 percentile, and peak (as defined in this report) lies on the 0.01 percentile. The median of the Rayleigh amplitude distribution is 1.6 dB below the mean while the peak is 9.6 dB above the mean. Impulsive noise is represented by amplitudes that exceed this line at low probabilities and continuous wave interference is represented by an approximately straight line with a slope that approaches zero as the continuous wave power to Gaussian noise power ratio increases.

1.1.4 Average Noise Power

White Gaussian noise is completely described by its variance, which is equivalent to the average noise power. The average noise power is vitally important for non-Gaussian noise also. The *average noise power* is the defined as

$$w_0 = E\{w\} \tag{1.9}$$

where $E\{\}$ denotes the expected value of its argument. The *average noise power* relative to kT_0b is called the *noise factor* and is given by

$$f = \frac{w_0}{kT_0b} , \tag{1.10}$$

and the *noise figure* in dB is

$$F = 10\log_{10} f. \tag{1.11}$$

1.1.5 Antenna Noise Factors

The noise collected by the antenna originates, presumably, from widely scattered directions at or near the horizon and is therefore altered by the receiving station antenna directional gain. If $S(\mathcal{2},\mathcal{N})$ is the power density coming from elevation $\mathcal{2}$ and azimuth $\mathcal{N}$, and $g(\mathcal{2},\mathcal{N})$ is the antenna directional gain relative to isotropic, then the total noise power received by an antenna is

$$w_a = \frac{\lambda^2}{4\pi} \int_0^{2\pi} \int_{-\pi/2}^{\pi/2} S(\theta,\phi) g(\theta,\phi) \cos(\theta) d\theta \, d\phi \tag{1.12}$$

where λ is the wavelength. The corresponding antenna noise factor is

$$f_a = \frac{E\{w_a\}}{kT_0 b} \ . \tag{1.13}$$

A noise power measurement system consists of an antenna, antenna matching circuit, transmission line, and receiver. If the antenna matching circuit and transmission line are assumed to be lossless and operating at a temperature T_0 , the measured noise factor is related to the antenna noise factor and receiver noise factor by

$$f_a = f - f_r + 1 \tag{1.14}$$

where f is the measured noise factor and f_r is the receiver noise factor. The corresponding antenna noise figure, the principle quantity used by radio system designers, is

$$F_a = 10\log_{10} f_a \ . \tag{1.15}$$

1.1.6 Statistics of Antenna Noise Figure

The statistical behavior of F_a can be shown by plotting the distribution on a *normal probability graph* where random variables that are Gaussian distributed form a straight line with a slope equal to its standard deviation and a median equal to its mean. The graph is used to determine the median antenna noise figure F_{am} of a *rural, residential, or business environment*. Further analysis of F_a includes determining *within-the-hour-, hour-to-hour-,* and *location-to-location*-variability.

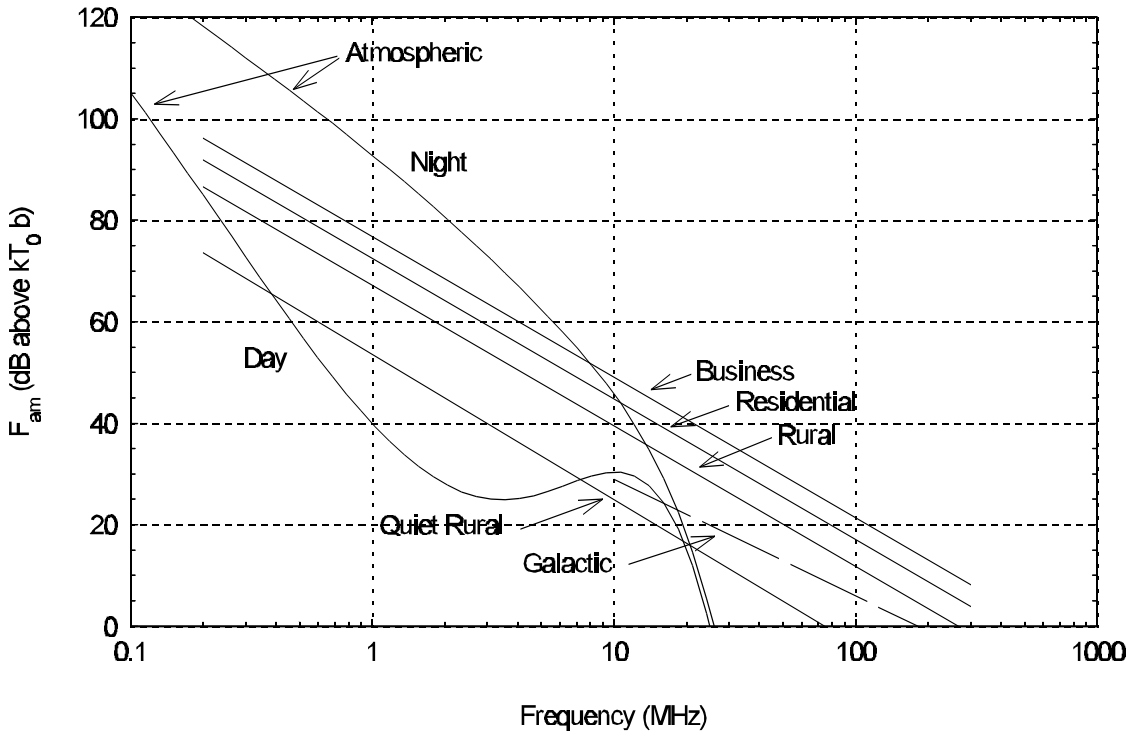

Figure 1.1 Median values of F_a

2. MEASUREMENT SYSTEM DESCRIPTION

The mobile noise measurement system (NMS) consists of a computer, receiver, antenna, and vehicle. This section describes the design and operation of the NMS.

2.1 Vehicle

Noise measurements were conducted at many sites over a wide geographic range in the Denver metropolitan area. For convenience, all measurements were obtained with the NMS installed in a vehicle. The vehicle is an extended-length van powered by a diesel engine. An aluminum sheet was welded to the top of the van to serve as a ground plane for the antenna. Instrument racks were installed in the rear of the van to hold measurement equipment.

2.1.1 Vehicle Power Sources

The power to the instruments was supplied directly from a 120-V ac connection or indirectly by a power inverter. The power inverter produced 120-V ac from the van 12-V dc power system (diesel engine, alternator, voltage regulator, and batteries).

The ac connection was preferred over the power inverter for two reasons. First, the ac connection could provide continuous power for extended measurement periods while the measurements made using the power inverter were limited in time by the size of the van fuel tank. The power inverter also added a small amount of radiated radio frequency interference (RFI) to the measurement results.

2.2 Antenna

Man-made noise is expected to arrive at the horizon from widely scattered directions. The effect of the directional gain on noise power measurements has been of concern [3,8] and has led to suggestions that there should be a standard measurement antenna. The standard most often suggested is a simple, short monopole antenna. This is a good choice at frequencies less than 30 MHz; however, at higher frequencies a more effecient quarter-wave monopole is a better choice.

The quarter-wave monopole antenna used for these measurements was mounted on a rectangular aluminum ground plane attached to the roof of the measurement van. The ground plane dimensions are 3.6m by 1.6m, or 1.64λ by 0.73λ at 137MHz where λ is the 2.19 m wavelength.

The quarter-wave monopole antenna pattern is dependant upon the size and shape of the ground plane [9]. A quarter-wave monopole antenna mounted on this ground plane will not have a perfectly omnidirectional antenna pattern; however, the distorted azimuth antenna pattern is not expected to significantly impact measurements. Of more concern was the elevation antenna pattern.

Finite-difference time-domain techniques were used to estimate the elevation antenna pattern. Figure 2.1 depicts the elevation antenna pattern for a quarter-wave monopole antenna mounted on a circular ground plane for three different radii representing the ground plane width (ka = 2.3), length (ka = 5.2), and a point in between (ka = 3.7), where a is the radius and k is $2\pi/\lambda$. The gain is approximately unity at the horizon for all cases; hence the ground plane size and shape is not expected to significantly impact the measurements.

Like the antenna pattern, the impedance of the quarter-wave monopole antenna depends on the size and shape of the ground plane. The mounted antenna voltage standing-wave ratio is 1.2 with a corresponding transmission loss of 0.04 dB. This measurement shows the impedance of the mounted antenna is well matched to the receiver input impedance.

2.3 Receiver

A custom receiver was built to ensure that wideband noise would not saturate receiver components and interference from other services would be minimized. The receiver has a noise figure of 2.9 dB and a center frequency of 137.0 MHz. The receiver could be tuned over the entire 136.0 to 138.0 MHz VHF meteorological satellite band.

The single conversion superheterodyne design is composed of rf, IF, and video detection stages. Figure 2.2 shows all components used in the receiver construction. Appendix A lists specifications of the components.

2.3.1 The rf Stage

A three-pole Chebyshev preselection filter, F1, with a 4.1-MHz, 3-dB bandwidth rejects the image frequency and strong out-of-band interferers prior to preamplification. A low-noise, high-gain preamplifier, A1, establishes receiver sensitivity. After preamplification, a five-pole Chebyshev image-stripping filter, F2, attenuates noise at the image frequency.

A double balanced mixer driven by a frequency synthesized local oscillator (LO) signal downconverts the signal to a 10.7 MHz IF. A double balanced mixer with a high 1-dB compression point minimizes the introduction of nonlinear effects. The frequency synthesizer has excellent frequency stability and low phase noise.

2.3.2 IF Stage

A low-pass filter (LPF), F3, with a 70-MHz 3-dB cutoff frequency rejects undesirable mixer products that may overload the first IF amplifier. A 10-dB pad, at the input of F3, ensures that reflected signals are attenuated.

The first IF amplifier, A2, boosts the signal before the first IF bandlimiting filter. The first IF filter, F4, has a three-pole Chebyshev response and a 214-kHz 3-dB bandwidth. Reducing the bandwidth from 4.1 MHz to 214 kHz reduces noise power and adjacent channel interference prior to further IF amplification. The 10-dB pad before this filter ensures that reflected signals are attenuated.

The next two amplifiers, A3 and A4, and 6-dB pad, P3, were used to adjust IF gain to correspond to the dynamic range of the log amplifier. The receiver IF gain was designed to measure 16 dB below and 64 dB above the average receiver input noise power.

The final IF bandlimiting filter, F5, is a six-pole Chebyshev crystal filter with a 32-kHz 3-dB bandwidth. This filter was chosen so that all noise measured would be within the APT satellite frequency allocation [10]. The filter noise equivalent bandwidth is approximately 34 kHz. The 10-dB pad, P4, before this filter ensures that reflected signals are attenuated.

2.3.3 Video Detection Stage

A log amplifier (LA) with a dynamic range of 80 dB was used for detection. The log amplifier has a rise and fall time of 700 ns and a 3-dB bandwidth of approximately 6 MHz. The maximum input signal is 0 dBm and the minimum input is -80 dBm. The maximum signal generates 2.2 V and the minimum signal generates 0.1 V. The slope of the log amplifier is 26.25 mV/dB. The log amplifier output is dc coupled so that a continuous wave signal can be used for power calibration.

2.4 Data Acquisition

An industrial computer housed in a metal, shielded case was used for data acquisition. The processor and bus speeds were 133 MHz and 66 MHz, respectively. The computer digitized, stored, and displayed noise power samples and their statistics.

2.4.1 Digitization

The output of the log amplifier was connected to the computer analog-to-digital conversion (ADC) card. The ADC card sampled the voltage at the log amplifier output 1000 times a second. The ADC card has 12 bits that cover 0-10 volts or 2.442 mV/ADC unit. The log amplifier slope is 26.25 mV/dB therefore our amplitude precision was approximately 0.1 dB.

2.4.2 Noise Histograms

Saving every noise power sample would have required tremendous amounts of computer data storage. To alleviate this problem, noise power samples were stored in 1000 histogram bins. The bins had a resolution of 0.1 dB and a range that extended from 26 dB below to 74 dB above the average receiver input noise floor. Each noise histogram contained 60,000 noise power samples that required approximately 60 seconds to digitize, and 50 seconds to develop into a histogram, record, and display on the screen.

2.4.3 Graphical User Interface

As the data were collected, two graphs were visible to the user. The first graph showed the recently acquired noise power samples while the second graph showed the last complete noise histogram.

2.5 Radio Frequency Interference

2.5.1 Radiated Radio Frequency Interference from Out-of-Band Interferers

The superheterodyne receiver may give erroneous results because of intermodulation products from strong out-of-band interferers or failure to properly attenuate image frequency signals. These possibilities were minimized by the proper selection of rf and IF filters and amplifiers. A spectrum survey conducted by ITS was examined to determine out-of-band attenuation requirements [11]. Out-of-band interferer- and image-rejection was measured with a continuous wave signal injected into the receiver input.

2.5.2 Radiated Radio Frequency Interference from NMS

Radiated radio frequency interference (RFI) was found to originate from the computer and power inverter. To suppress this RFI, Type 43 ferrites were placed on all cables coming out of their metal

cases and van doors were closed during measurements. Radiated RFI was measured with an antenna in a radio-quiet canyon with the computer and power inverter turned on.

2.5.3 Conducted Radio Frequency Interference

Conducted RFI originating from the ac connection or power inverter was attenuated by power line filtering. Conducted RFI was measured by replacing the antenna with a 50-ohm termination. Conducted RFI was never observed in any of these measurements.

2.6 Verification

The NMS operation was verified with the following measurements: noise power measured with 50 ohm receiver input termination, noise power measured with antenna in a radio-quiet canyon, and continuous wave interference power measured with a continuous wave signal injected at the receiver input.

Figure 2.3 shows median, mean, and peak powers measured with a 50-ohm receiver input termination over a 24-hour period. This measurement was performed to assure measurement repeatability over changing temperatures. Figure 2.4 shows an APD during this extended measurement. This APD indicates that receiver noise is Gaussian.

Figure 2.5 shows an APD obtained with the antenna in a radio-quiet canyon. The van is operating with its power inverter. The mean of this measurement is less than 1 dB higher than the mean with the 50-ohm load.

Figure 2.6 shows an APD obtained with a signal generator connected to the receiver input. The signal generator injected a continuous wave signal with 10 dB more power than the receiver average noise power. The measured APD corresponds to the APD of a Nakagami-Rice distribution with a K factor of approximately 10 dB as expected.

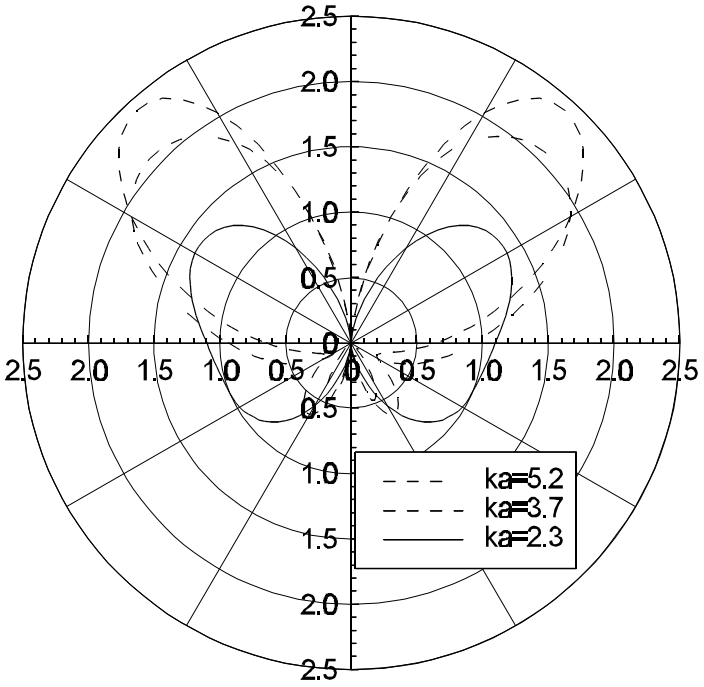

Figure 2.1 Antenna pattern of a quarter-wave monopole antenna over a circular ground plane.

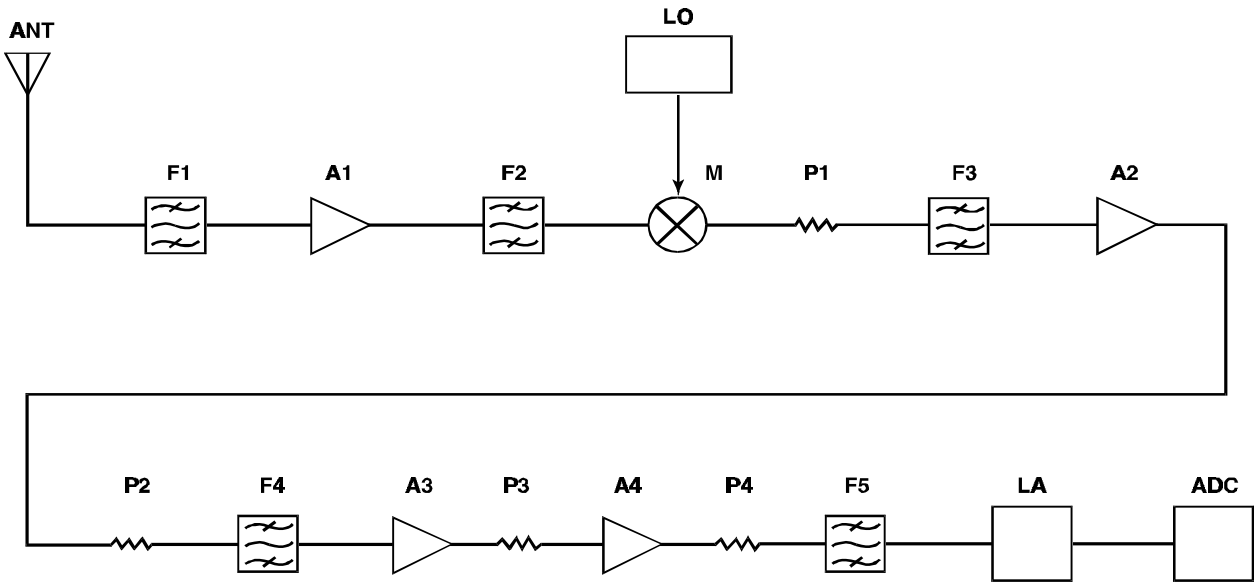

Figure 2.2 Receiver block diagram.

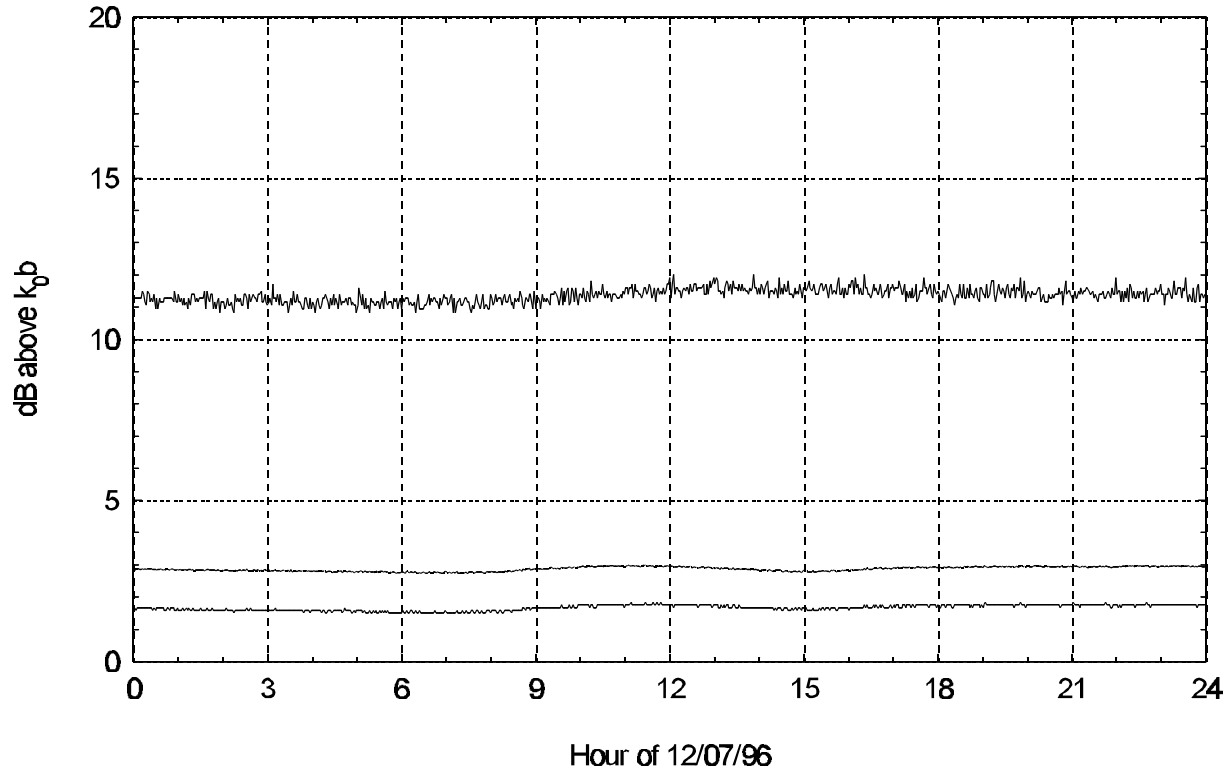

Figure 2.3 Median (bottom), mean (middle), and peak (top) receiver noise power over a 24-h period.

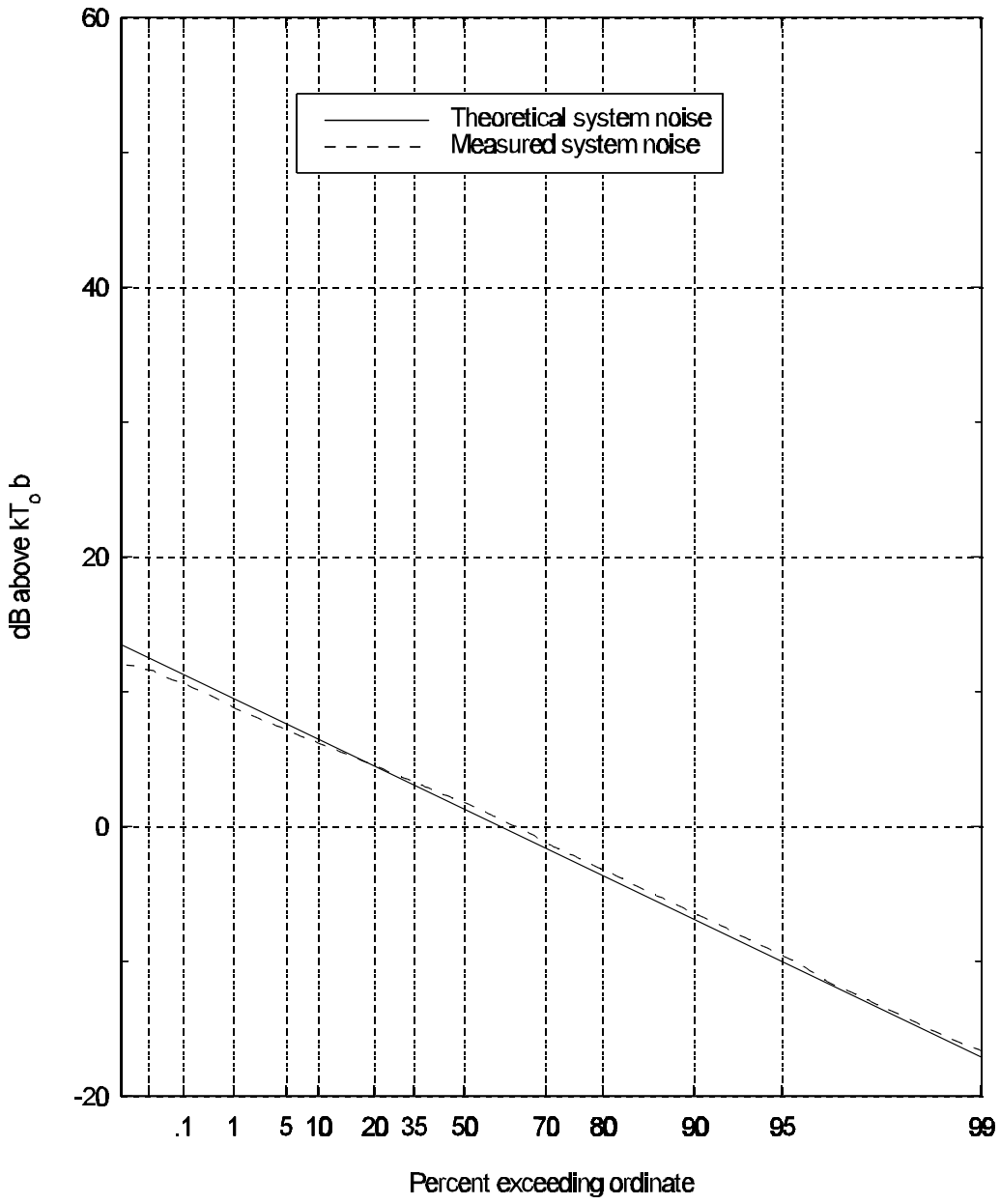

Figure 2.4 APD of receiver noise power.

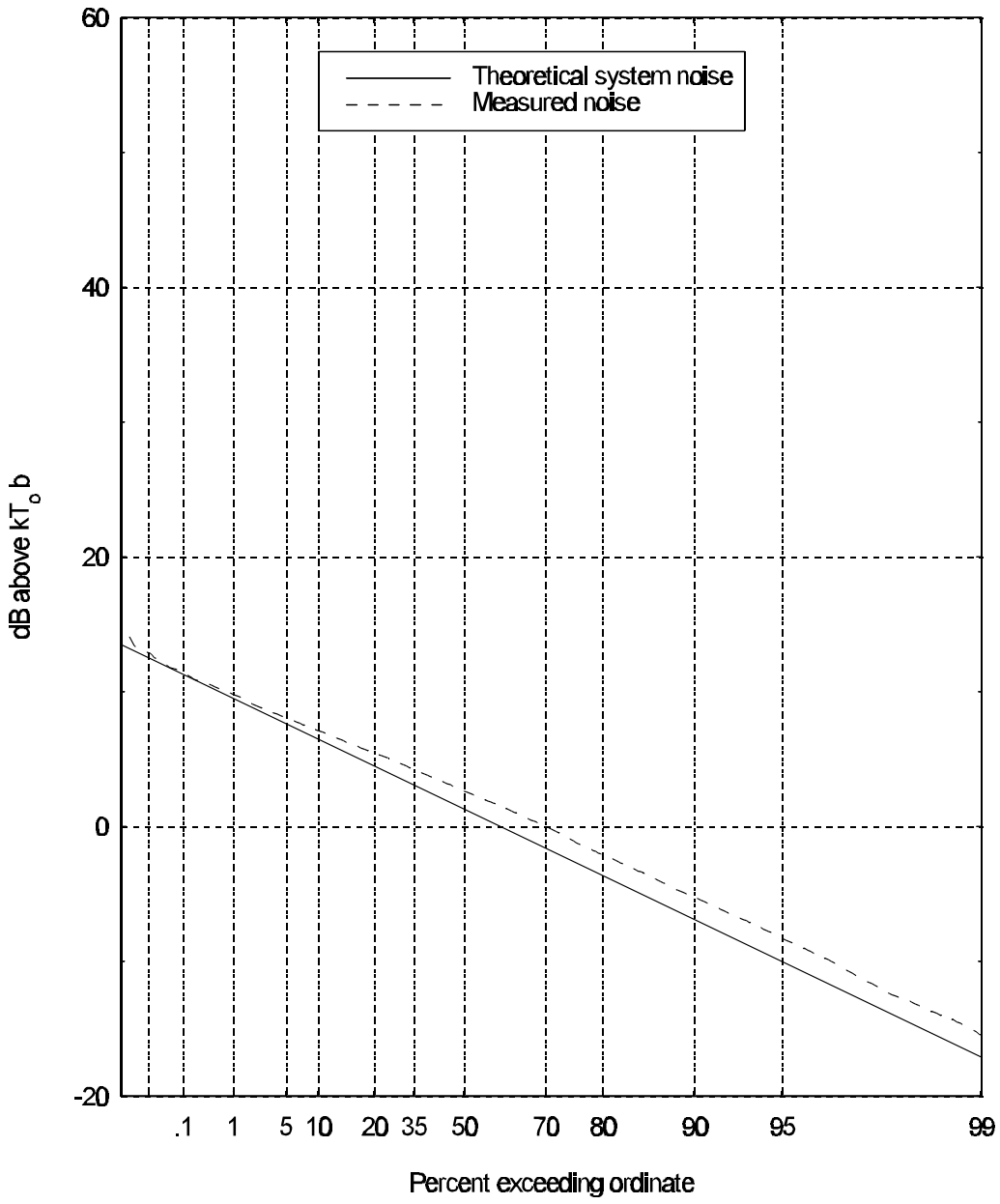

Figure 2.5 APD of environmental noise in a quiet canyon with power inverter on.

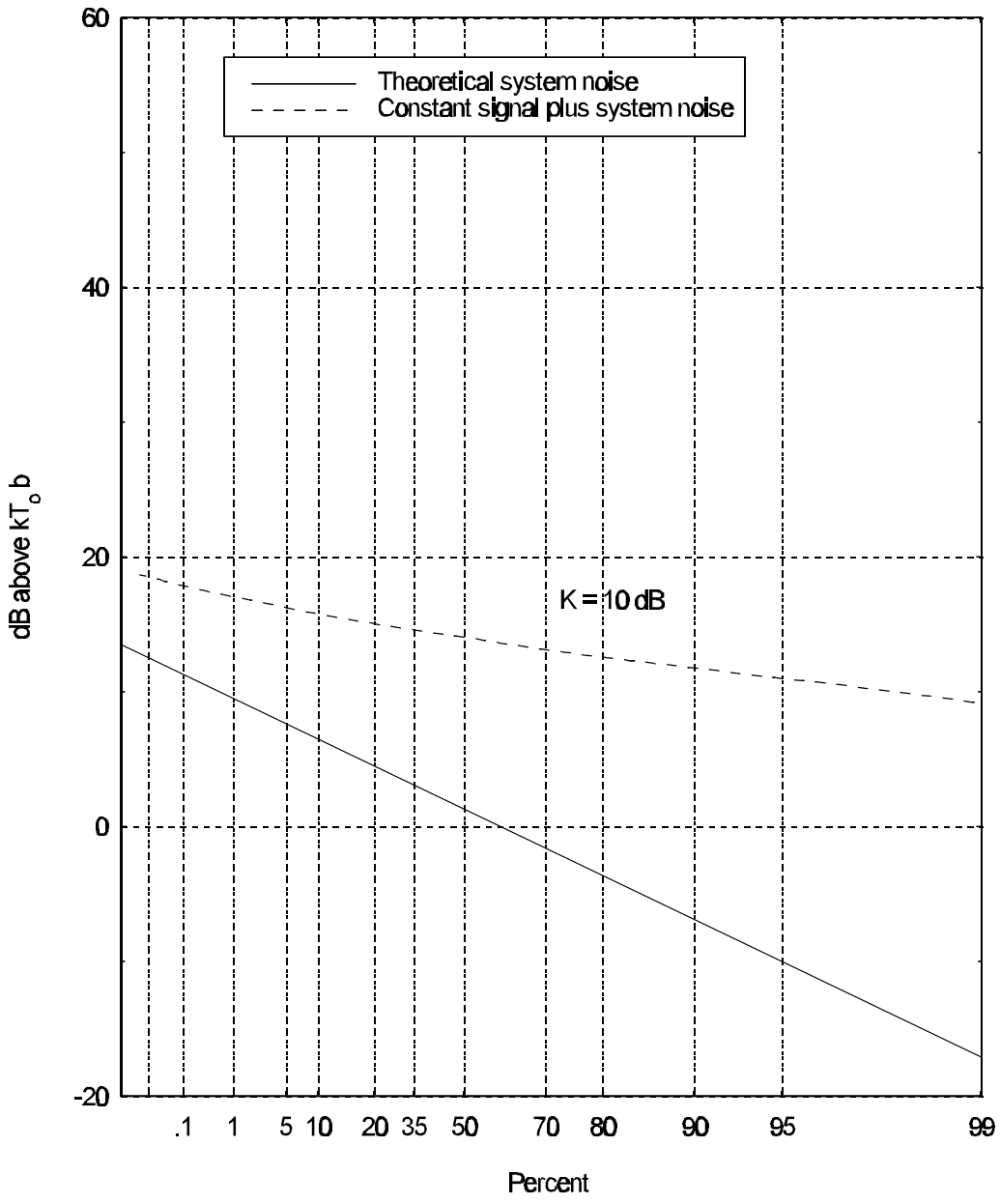

Figure 2.6 APD of a continuous wave signal with a 10-dB signal-to-noise ratio.

3. MEASUREMENTS

In this section the measurement procedure is described and representative measurements are summarized.

3.1 Procedure

All measurements were obtained while the van was parked. All doors to the van were closed during measurements to maximize shielding from radio frequency interference (RFI) generated by the NMS equipment. If possible, the van was powered with an ac connection; otherwise the van power inverters were used. After the instruments had warmed up, a series of tests were conducted to ensure the system was operating properly.

First, the antenna was replaced by a 50-ohm load. The log amplifier output was connected to a digital oscilloscope to measure the noise power and determine if any conducted RFI was present. The log amplifier output then was connected to the ADC and one or more noise histograms were collected for calibration purposes. Next, the antenna was reconnected and the preamplifier output was connected to the input of a spectrum analyzer to look for interference.

The measurements were conducted at the 137.5 MHz APT satellite frequency allocation. We chose to operate at this frequency so that the measurements would be protected from other satellite transmitters. We also were able to use the APT signal to verify receiver operation. The satellite was visible every 12 hours when it would make three passes that were 15 minutes in duration, at 100-minute intervals. The frequency modulated satellite signal was evident in the noise power measurement data when mean and median powers rose, converged, fell, and diverged in time intervals corresponding to the three satellite passes. Figure 3.1a illustrates three satellite passes at 5:30 a.m., 7:15 a.m., and 9:00 a.m.

3.2 Representative Noise Measurements

Representative noise power measurements are summarized graphically by showing the median, mean and peak (value exceeded 0.01% of time) powers in dB relative to kT_0b for each measured histogram over time. The median, mean, and peak powers are the bottom, middle, and top curves respectively of these graphs. Noise added by the receiver has not been removed from these values; therefore, the mean corresponds to the measured noise figure, F. All measurements shown were taken from September 1996 to February 1997.

3.2.1 Residential Noise Measurements

The first residential site is located in a Lakewood, Colorado, subdivision built in the 1960's. The nearest business is approximately 1 km away and the nearest major road also is approximately 1 km away. Measurements were obtained over a 4-day period from Friday, November 8, to Tuesday,

November 12. Two complete days, Sunday, November 10, and Monday, November 11, are shown in Figure 3.1.

The two days show similar median, mean, and peak power behavior. The median power was constant throughout both days. The mean power was fairly constant; however, it was occasionally affected by the peak power. During both days, the peak power was constant from 20:00 to 08:00 the next morning; however, during the day the peak power was variable. The drop of the peak power during the day on Monday, November 11 is dramatic in comparison to Sunday, November 10.

The second residential site is located in a Boulder, Colorado, subdivision built in the 1950's. The nearest business is approximately 1 km away and the nearest major road also is approximately 1 km away. Measurements were taken over a 3-day period from Friday, November 15, to Monday, November 18. Two days of measurements are shown in Figure 3.2.

Before 7:00 on November 17, median and mean power were fairly constant. After 7:00 the median, mean, and peak power rose and stayed at the increased level until 10:00 November 18, when the measurement was stopped. The weather on November 16 was snowy, cold, and cloudy while November 17 was clear, warm, and sunny.

3.2.2 Business Noise Measurements

The office park consisted of several four-story office buildings in Golden, Colorado, located between a major interstate highway and a residential area. The electrical distribution lines are buried. Three extended measurements were conducted at the park. The first measurement location was at the edge of the office park near an interstate highway and approximately 200 m from the nearest office building. The measurements began on Friday, November 22, and ended Tuesday, November 26. Figure 3.3a shows the results from Monday, November 25, at this location. At 00:30 median, mean, and peak powers were very low. The peak power increased slightly until 04:00 with very little effect on the mean power. From 04:00 until 15:00 the median, mean, and peak power increased slowly. After 15:00 all three powers decreased.

The next measurement location was in the center of the office park. The nearest office building was 15 m from the receiver, a road was within 10 m of the receiver, and a metal electrical utility closet was located 4 m from the receiver. The measurements began Tuesday, November 26, and ended Friday, November 29. Figure 3.3b shows the results from Wednesday, November 27, at this location. The median and mean power were the highest of the three measurements in the office park. The peak power indicates the noise was more impulsive in the day than during the night. The largest impulses corresponded to the beginning and end of the work day.

The last measurement location was at the edge of the office park near a residential area. The van was parked within 15 m of the office building and about 50 m from the residential area. A large heating ventilation and air conditioning (HVAC) motor was located 5 m from the receiver. The measurements began Friday, November 29, and ended Monday, December 2. Figure 3.3c shows the

results from Saturday, November 30, at this location. From 00:00 to 06:00 there were some large, regularly occurring peak values. This regularity was unique in the office park data set and is conjectured to be due to noise originating from the nearby HVAC motor.

The first downtown site was located at the intersection of 13th Street and Pearl Street in downtown Boulder, Colorado. This location is surrounded by one- and two- story office buildings and streets with heavy traffic. The measurement was conducted with inverter power because no ac connection was available.

The measurement, shown in Figure 3.4a, lasted approximately 3 hours from 11:40 to 14:40 Wednesday, November 20. The peak power was variable while the median and mean were fairly steady.

The second downtown site included three different locations in downtown Denver, Colorado. The longest duration measurement was obtained at the corner of 17th and Lawrence Street. This location is characterized by tall buildings and streets with heavy traffic. The measurement was conducted with inverter power because no ac connection was available.

The measurement, shown in Figure 3.4b, lasted approximately 3 hours from 10:15 to 13:15 on Tuesday, December 3. Median, mean, and peak power were very similar to those obtained in downtown Boulder, Colorado.

3.2.3 Rural Noise Measurements

Rural mountain noise levels were measured in a steep canyon near Ward, Colorado. At the measurement location there were no visible power lines or houses. A few cars passed by while the measurement was taken. The measurement, shown in Figure 3.5a, was conducted between 10:00 and 11:00 on Thursday, December 5. The results are characterized by constant median, mean, and peak power.

Rural plains noise levels were measured in rural eastern Colorado. The location is characterized by the absence of houses and power lines. Nearby roads have little or no traffic. The measurement was conducted with inverter power because no ac connection was available. The measurement, shown in Figure 3.5b, was conducted on Friday, December 6, from 13:15 to 15:15. The measurement shows fairly constant median, mean, and peak values. Rural plains values were very similar to rural mountain values.

3.2.4 Automotive Noise Measurement

Automotive ignition noise was measured on a road passing through Clear Creek Canyon between Golden, Colorado, and Black Hawk, Colorado. We parked the measurement van along the road at a place in the canyon with steep walls and no power lines or buildings so that we could be reasonably sure the only noise measured originated from automobiles. The measurements were conducted with

inverter power since no ac connection was available. The measurement, shown in Figure 3.6, was collected on Thursday, November 21, between 13:00 and 15:00. Median and mean values were fairly constant, while peak values varied.

3.2.5 Electrical Network Noise Measurement

Electrical utilities generate, transmit, and distribute electrical power throughout most business, residential, and rural areas. The transmission generally is performed at high voltage levels while distribution of the electrical power to buildings is performed at lower voltage levels. The noise attributed to the electrical network is generated by corona and gap discharge phenomena and has been studied for many years [12].

Noise from electrical transmission and distribution was measured on a lightly traveled road located between Highway 93 and the small town of Leyden, Colorado. A high-voltage transmission line runs perpendicular to this road, while a low-voltage distribution line runs parallel to the road. The road is located in the bottom of a gently sloping valley. The measurements were obtained with inverter power because no ac connection was available.

Three measurements, shown in Figure 3.6, were obtained along this road on Tuesday, November 12. The first measurement, obtained directly under the high-voltage line from 13:30 to 14:00, showed low mean powers. The second measurement, obtained about 70 m from the high-voltage transmission line from 14:30 to 15:30, was similar to the first. The third measurement; however, conducted approximately 2 km from the high-voltage transmission line from 15:45 to 16:30, showed a mean and peak power 15 to 20 dB higher than the previous two measurements. The third measurement was obtained in close proximity to an electrical distribution device mounted on a wooden pole.

3.2.6 Electronic Equipment Noise Measurement

Electronic equipment has proliferated since similar noise measurements were undertaken in the 1970's. Microprocessors with clock speeds of hundreds of MHz are embedded in many consumer items, not the least of which is the ubiquitous personal computer. During the measurement campaign we observed electronic equipment noise that was both broadband and narrowband in comparison to the bandwidth of the final IF filter of the measurement receiver.

The noise from two computers was measured in a relatively quiet area located in the Plainview Open Space near Boulder, Colorado. The computers tested were placed about 3 m from the receiving antenna. Three measurements, shown in Figure 3.8, were taken on Tuesday, December 10. First, noise from a 20-MHz clock speed personal computer was measured from 14:15 to 14:45; next, a background measurement without computers was obtained from 14:45 to 15:15, and last, noise from a 50-MHz clock speed personal computer was measured from 15:30 to 16:00.

These measurements show that computer noise varies considerably. These spikes in the mean and peak power of the background measurement were observed at other times at this location. We assumed it was coincidence that they were not present when either of the two computers was measured.

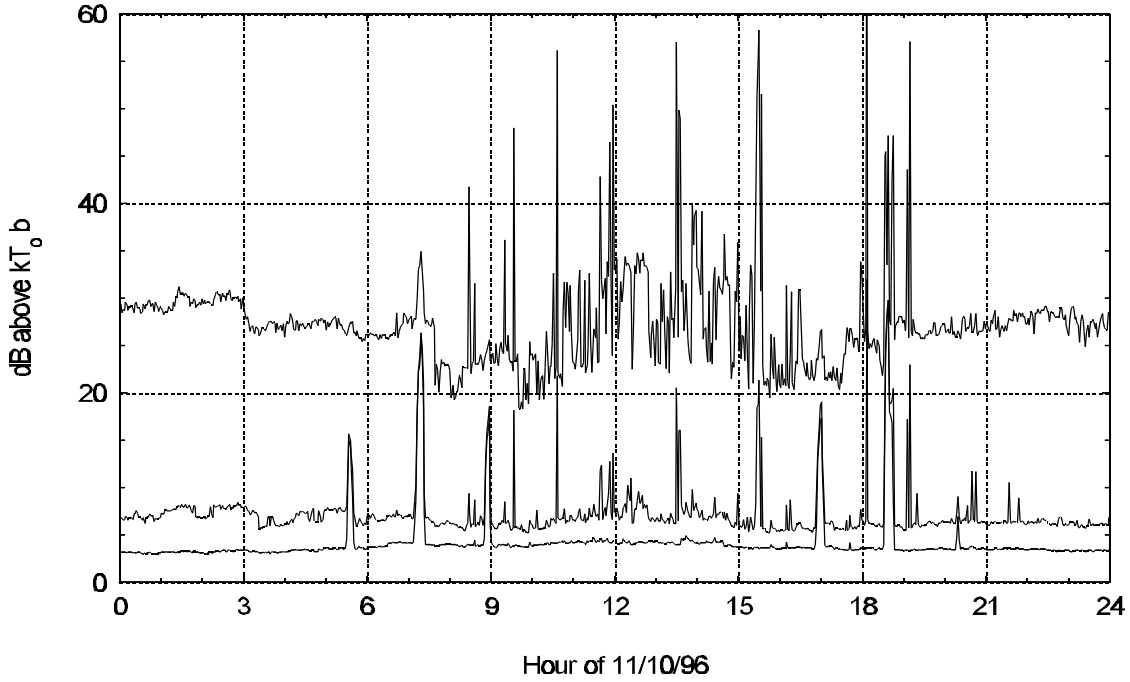

Figure 3.1a Median, mean, and peak power at Lakewood, Colorado, residence on November 10, 1996.

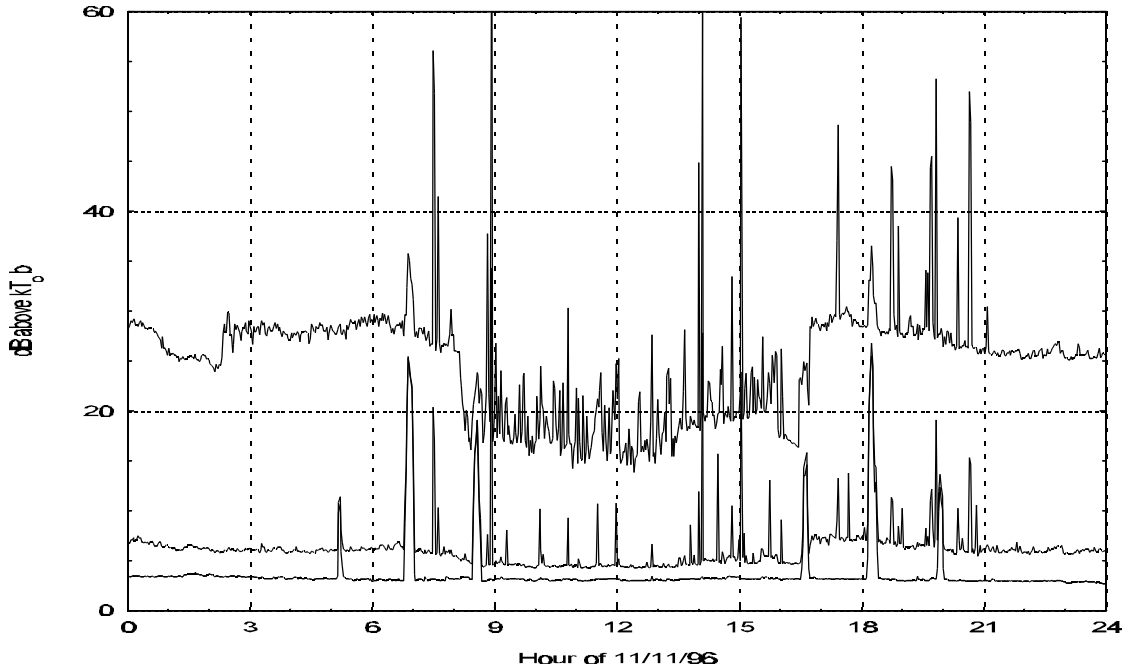

Figure 3.1b Median, mean, and peak power at Lakewood, Colorado, residence on November 11, 1996.

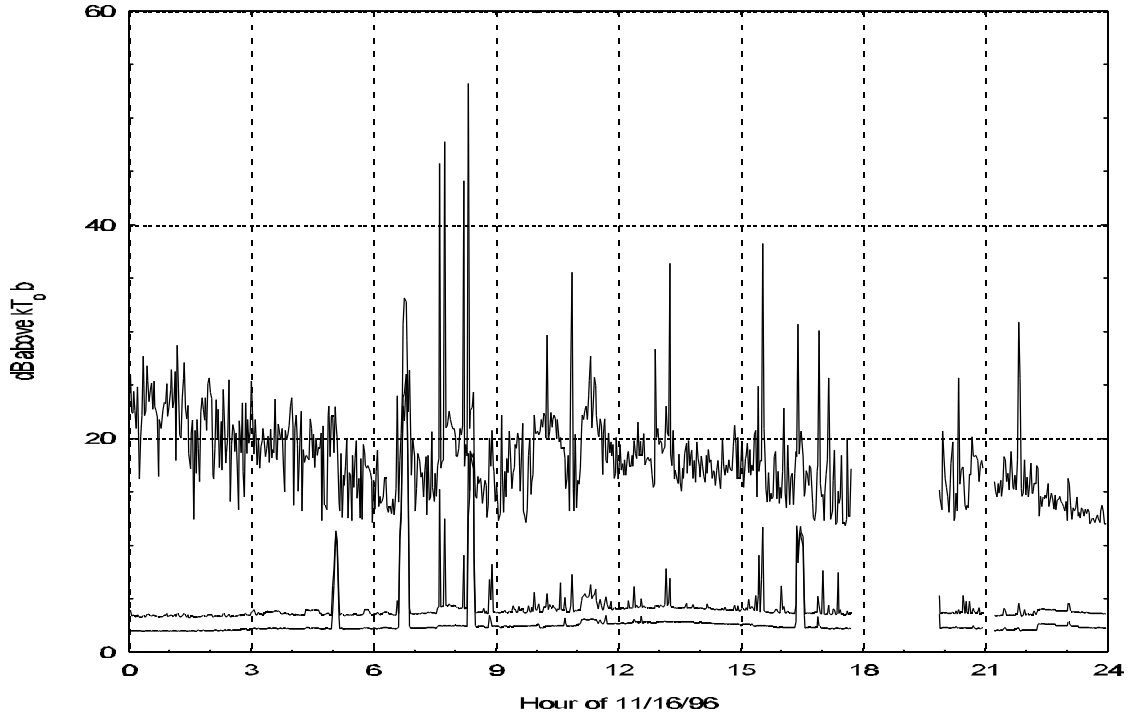

Figure 3.2a Median, mean, and peak power at Boulder, Colorado, residence on November 16, 1996.

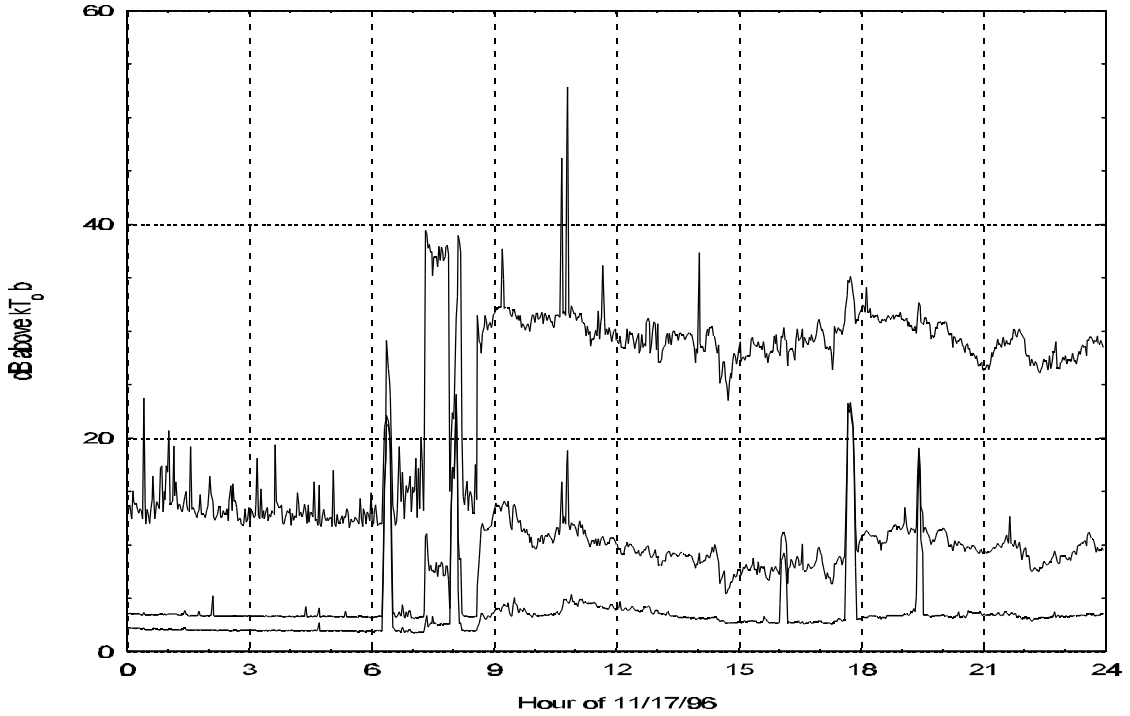

Figure 3.2b Median, mean, and peak power at Boulder, Colorado, residence on November 17, 1996.

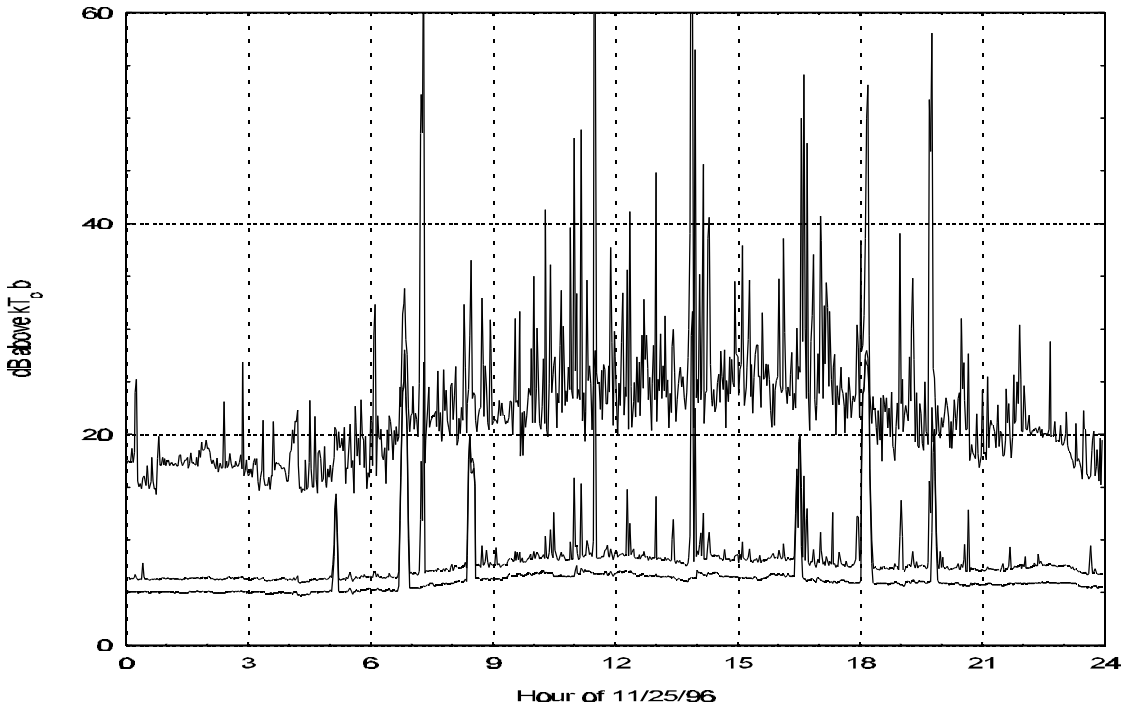

Figure 3.3a Median, mean, and peak power at edge of office park site near interstate highway on November 25, 1996.

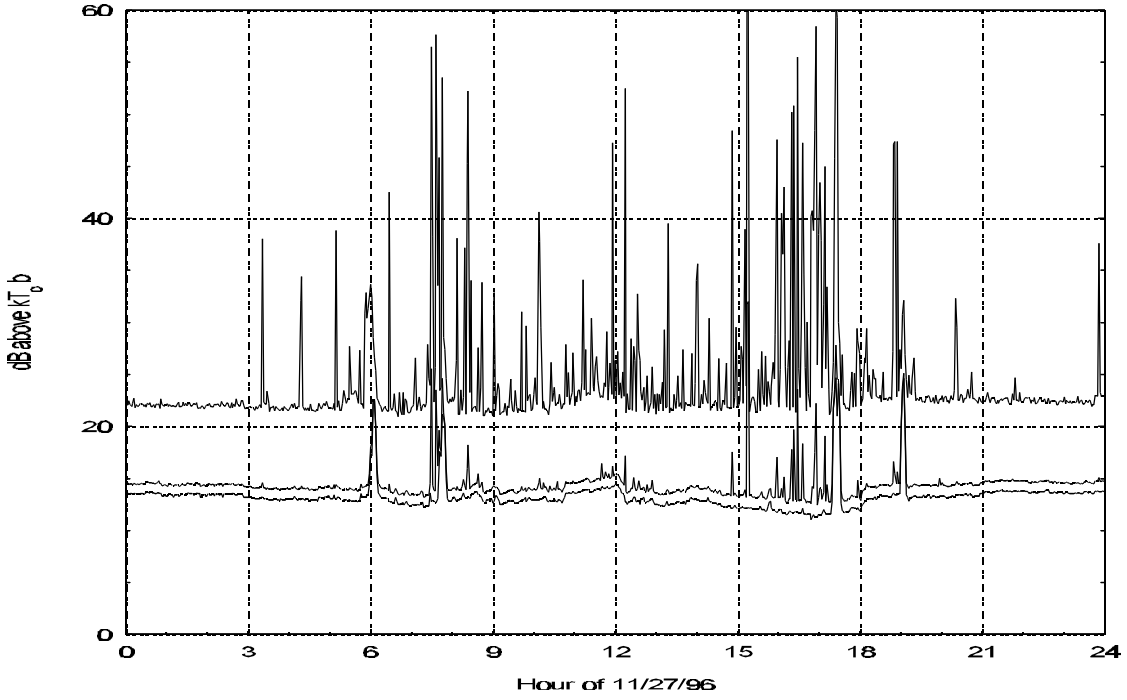

Figure 3.3b Median, mean, and peak power at center of office park site on November 27, 1996.

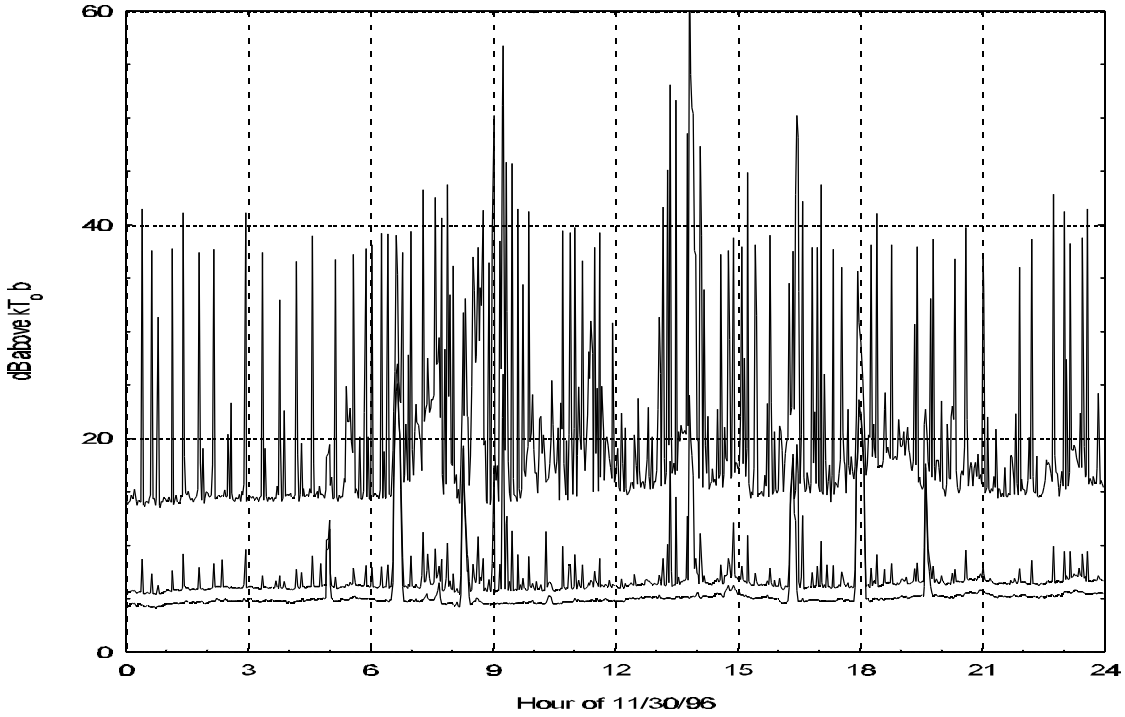

Figure 3.3c Median, mean, and peak power at edge of office park site near residential area on November 30, 1996.

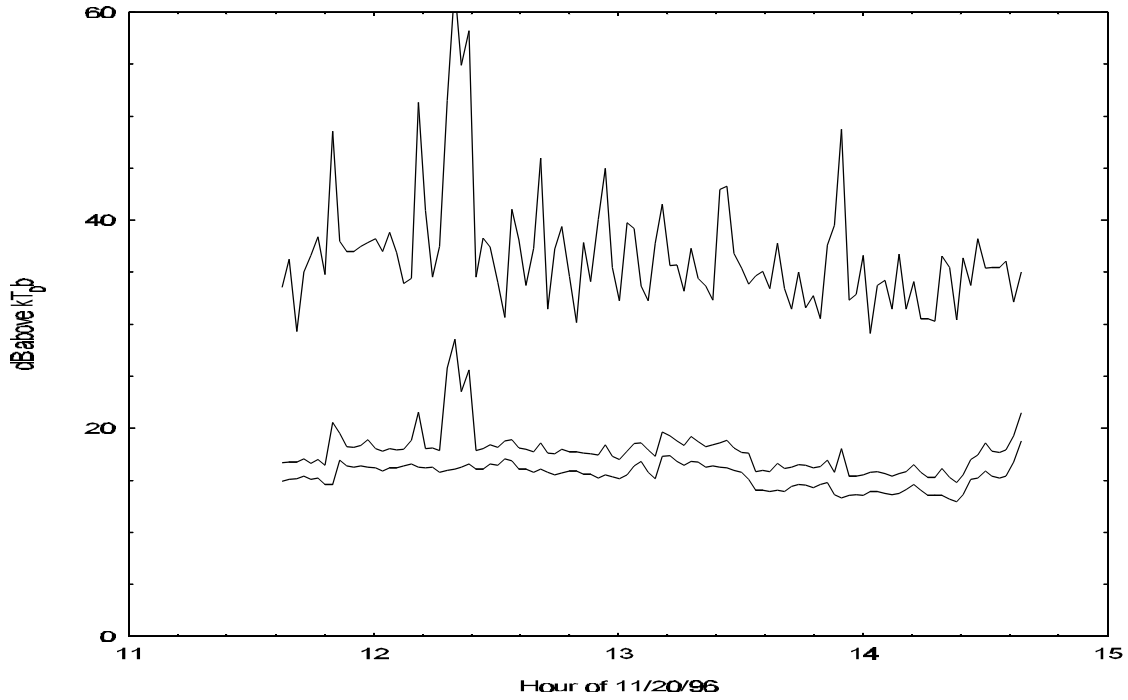

Figure 3.4a Median, mean, and peak power at downtown Boulder, Colorado, site on November 20, 1996.

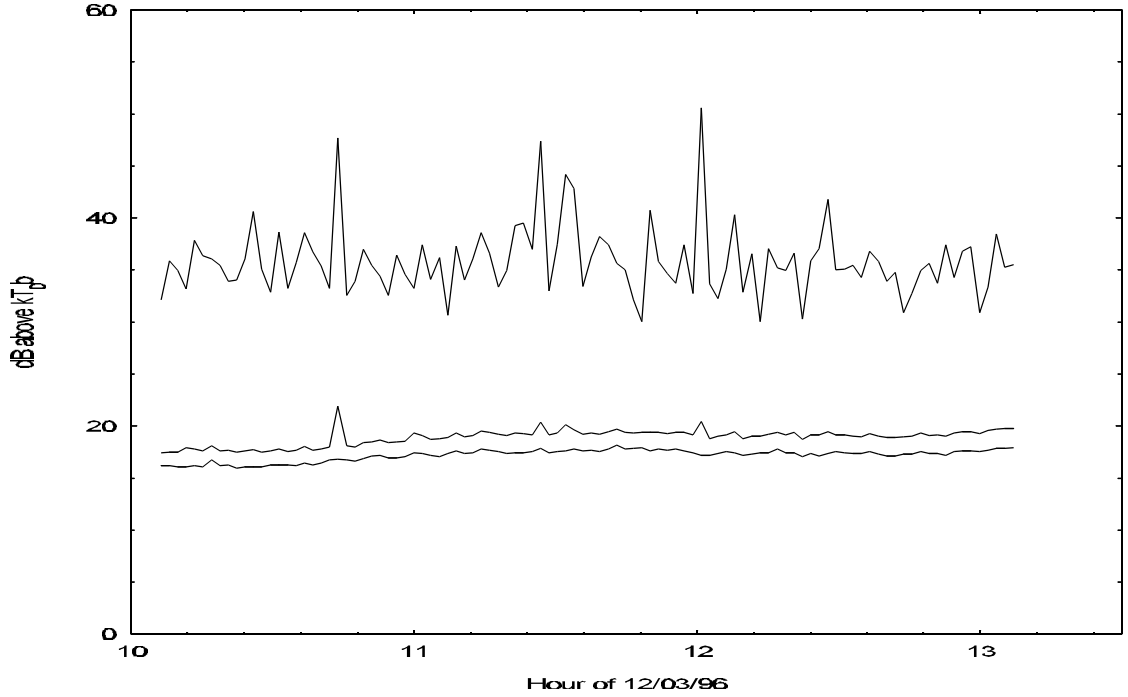

Figure 3.4b Median, mean, and peak power at downtown Denver, Colorado, site on December 3, 1996.

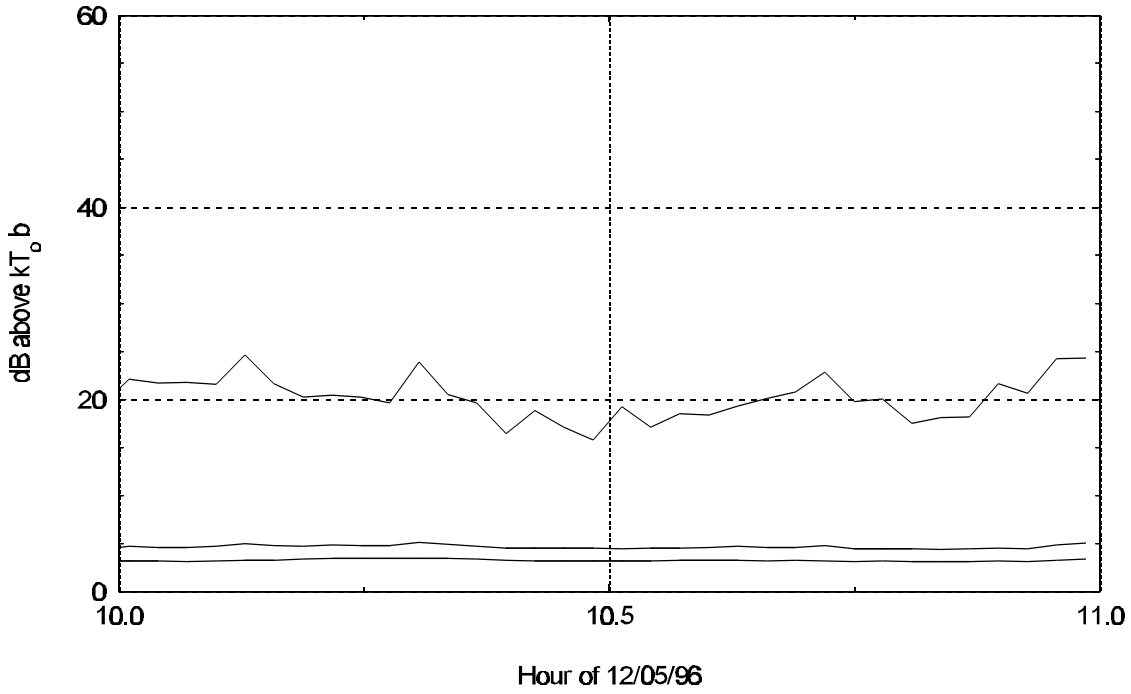

Figure 3.5a Median, mean, and peak power at rural mountain site near Ward, Colorado, on December 5, 1996.

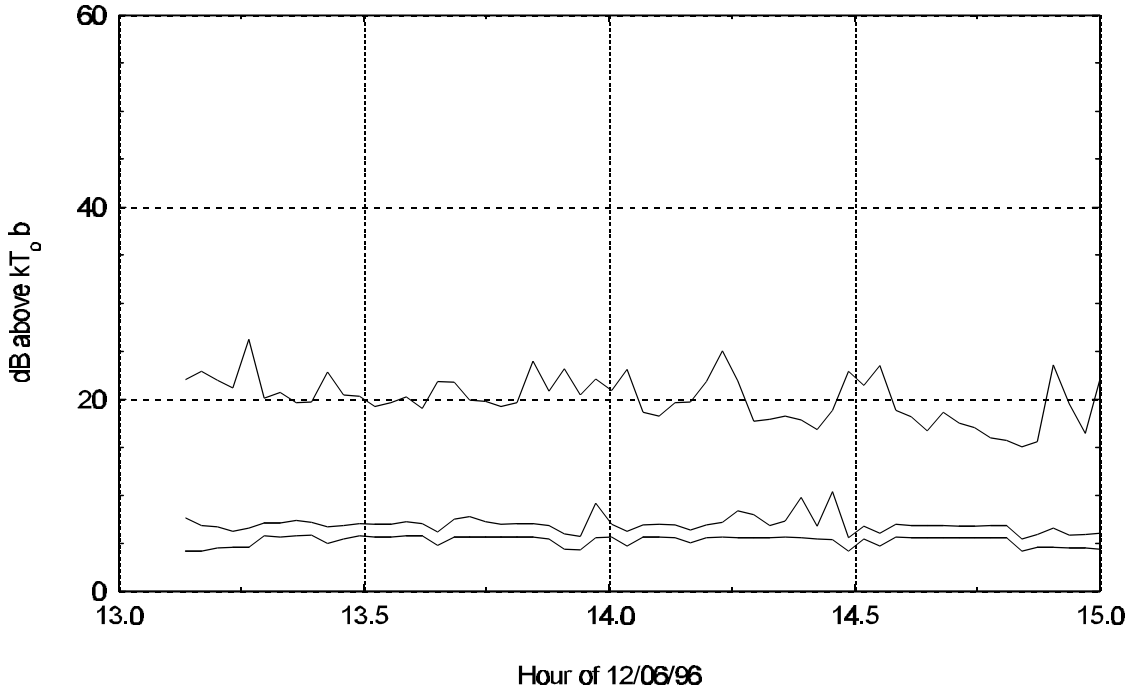

Figure 3.5b Median, mean, and peak power at rural plains site in eastern Colorado on December 6, 1996.

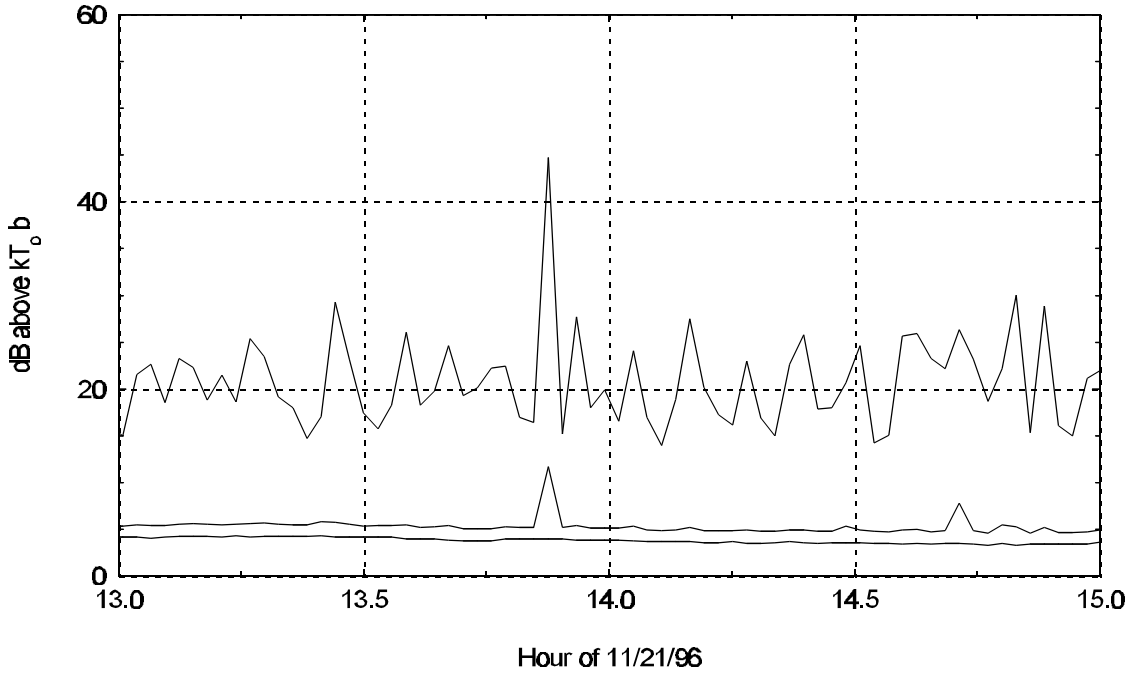

Figure 3.6 Median, mean, and peak power of automobiles measured in Clear Creek Canyon, Colorado.

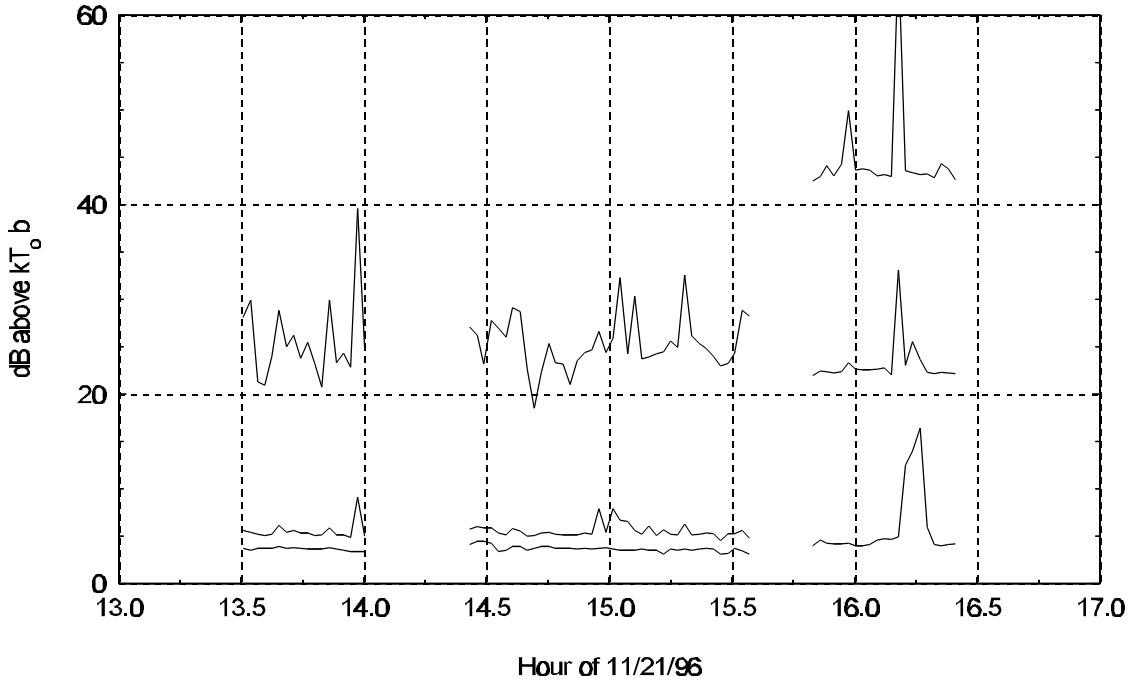

Figure 3.7 Median, mean, and peak power of electrical network measured near Leyden, Colorado.

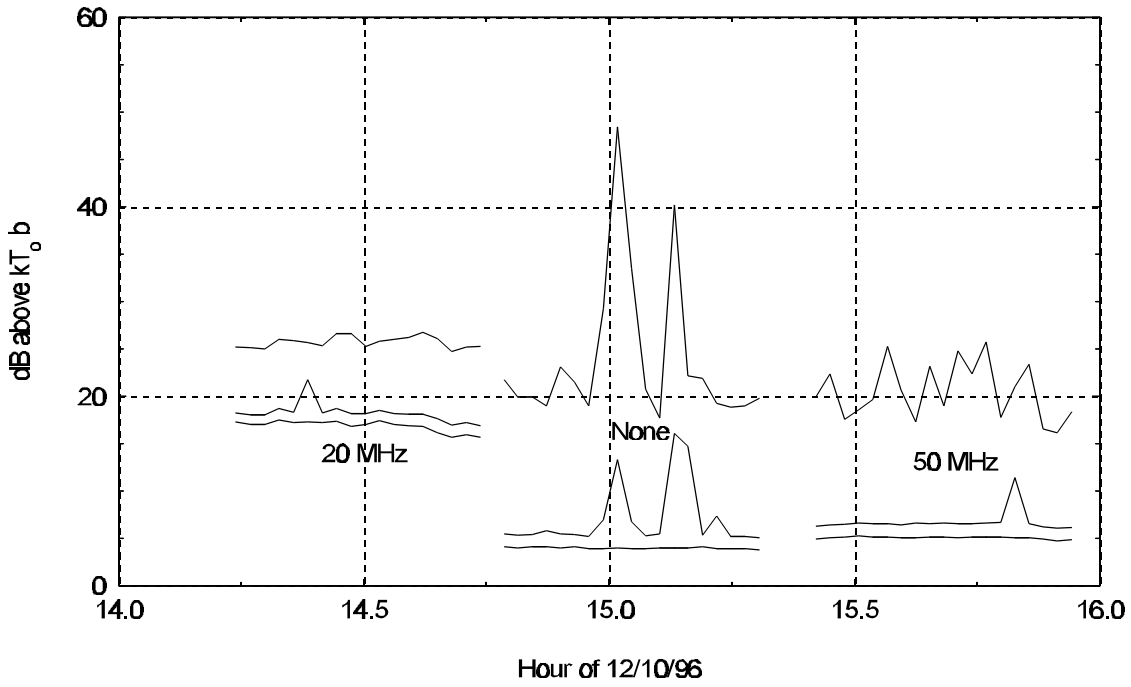

Figure 3.8 Median, mean, and peak power of computers measured at Plainview Open Space near Boulder, Colorado.

4. NOISE FIGURE SUMMARIES

In this section we present distribution functions of median, mean, and peak noise powers, we describe and compare the measurement and analysis methods to those used by the CCIR, and we conclude by contrasting the noise figure results with those used by the CCIR.

4.1 Distribution Functions of Median, Mean, and Peak Powers

We began our noise figure analysis by constructing distribution functions of median, mean, and peak powers for rural, residential, and business environments. These values were derived from measurement histograms spaced approximately one hour apart. The distribution functions were plotted on a normal probability graph where a Gaussian distributed variable is represented by a straight line whose mean lies on the 50th percentile and slope is the standard deviation. The distribution functions shows the probability that the median, mean, or peak exceeds a particular value.

The mean, in these plots, is the antenna noise figure, F_a, derived from

$$F_a = 10\log_{10}(f - f_r + 1) \tag{4.1}$$

where, recalling the notation in Section 1, f is the measured noise factor and f_r is the receiver noise factor. In a similar way the median value is

$$G_a = 10\log_{10}(g - g_r + 1) \ . \tag{4.2}$$

In this case g represents the measured median noise power and g_r represents the receiver median noise power. This correction is based on the somewhat dubious approximation [13] that the median of a convolution is the sum (or difference) of the two component medians. The peak value is uncorrected and represents the measured noise power in dB above kT_0b that is exceeded 0.01 percent of the time.

Figure 4.1 shows the distribution function of G_a , F_a , and peak power over a 4-day period at the Lakewood, Colorado, residential site described in Section 3. In Figure 4.2 we have plotted the F_a for both residential sites. Note how the median F_a varies for the two locations. Figure 4.3 shows the G_a , F_a , and peak power for the two residences combined.

Similarly in Figure 4.4 the distribution functions for the F_a of six business locations are displayed. There seems to be two populations - a noisy, “business” set and a quieter, “light urban” set. The center of the office park falls within the business set, while locations adjacent to interstate highways fall within the light urban set. Figures 4.5 and 4.6 show the G_a , F_a , and peak power for each population. Only measurements taken during working hours were used.

Figure 4.7 shows the combined data from four rural locations. All of the measurements included in the distribution were taken during working hours. Cummulative distribution functions for each rural

location are not shown because of the short measurement periods involved. While the peak is considerably less than that observed in other environments, it still exceeds Gaussian noise values. Thus, even in rural areas, there is impulsive noise.

4.2 Comparison of Measurement and Modeling Methods

4.2.1 Measurement and Analysis Methods used by CCIR

CCIR methods for predicting man-made noise factors are based on approximately 300 hours of noise measurements at 31 rural-, 38 residential-, and 23 business-environment "measurement areas" [1]. The measurements were obtained during "mobile runs" through the measurement area, which ranged in size from a few city blocks for a business environment to several square kilometers for a rural environment. The mobile run was typically made during working hours and lasted approximately one hour. Eight frequencies ranging from 250 kHz to 250 MHz were measured simultaneously.

The objective was to estimate each environment F_{am} defined as the average noise power that can be expected in 50% of the measurement areas for 50% of the time within-the-hour. To accomplish this objective the mobile runs were sorted according to environment, and the median F_a of each mobile run was determined. Since the mobile runs lasted approximately one hour this median represented the hourly median F_a. The hourly median F_a values were plotted as a function of frequency, and a linear regression line representing the environment F_{am} across the frequency range was determined. A similar procedure was used to determine the environment within-the-hour upper and lower deciles of F_a represented by D_u and D_l, respectively.

The standard deviation of the hourly median F_a values from the environment F_{am} value is defined as the *location variability*, σ_L. The D_u and D_l can be combined to represent the *within-the-hour time variability*

$$\sigma_T = \frac{1}{1.28}\left[\frac{D_u^2 + D_l^2}{2}\right]^{\frac{1}{2}} . \tag{4.3}$$

Finally the *composite variability* represents the location- and within-the-hour time- variability

$$\sigma_c = \sqrt{\sigma_L^2 + \sigma_T^2} . \tag{4.4}$$

Using these parameters, the behavior of F_a can be modeled by

$$F_a = F_{am} + y_L(l) + y_T(t) . \tag{4.5}$$

where y_L and y_T represent location and time deviations, which are zero-mean Gaussian distributions with standard deviations of σ_L and σ_T, respectively.

4.2.2 Measurement and Analysis Method Used by this Study

We analyzed approximately 100 hours of noise measurements in 4 rural-, 2 residential-, and 6 business-environment locations. Our measurements were obtained while the measurement van was parked and only noise at a single frequency was measured. Rural measurement durations were typically less than an hour, residential measurement durations were often more than 24 hours, and business measurement durations varied from 1 to more than 24 hours.

Our measurements indicated that F_a changed little within the hour. This is in contrast to the 6.6 dB σ_T, independent of environment or frequency, reported by Spaulding and Stewart [14]. One consequence of a negligible σ_T is that it was not necessary to determine the hourly median F_a of a location. Instead, sampling F_a once per hour (avoiding satellite passes) is sufficient for any location. The distributions of the sampled F_a are shown in Figures 4.3, 4.5, 4.6, and 4.7. The median of the sampled F_a represents the median over all hours and locations measured. This median can be compared to the F_{am} used by the CCIR methods. The standard deviation of the sampled F_a can be compared to CCIR method σ_L since σ_T was negligable.

4.3 Noise Figure Predictions.

Table 1 shows our measured F_{am} and σ compared to values in CCIR Recommendations. Business and rural environment F_{am} fall within one standard deviation of CCIR Recommendations; however, residential F_{am} has decreased dramatically and is more than two standard deviations from CCIR Recommendations. This indicates that residential noise power may have decreased.

Table 1. Measured Noise Figure Statistics Compared to CCIR Recommendations at 137 MHz

Environment	**Measured**		**CCIR Recommendations**	
	F_{am} (dB)	**σ (dB)**	**F_{am} (dB)**	**σ_L (dB)**
Business	18.0	2.6	17.6	8.0
Light Urban	8.5	5.8	----	----
Residential	6.0	2.9	13.3	2.7
Rural	6.3	1.5	8.0	3.2

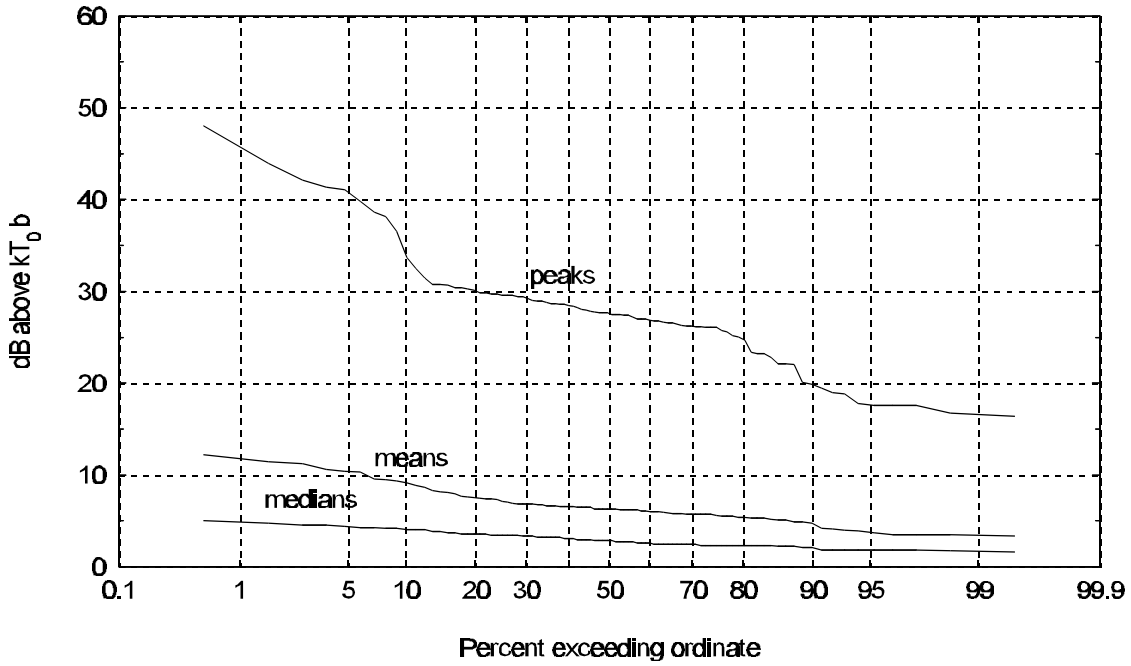

Figure 4.1 Cummulative distribution functions of the median, mean, and peak values for a 4-day sequence of measurements at the Lakewood, Colorado, residential location.

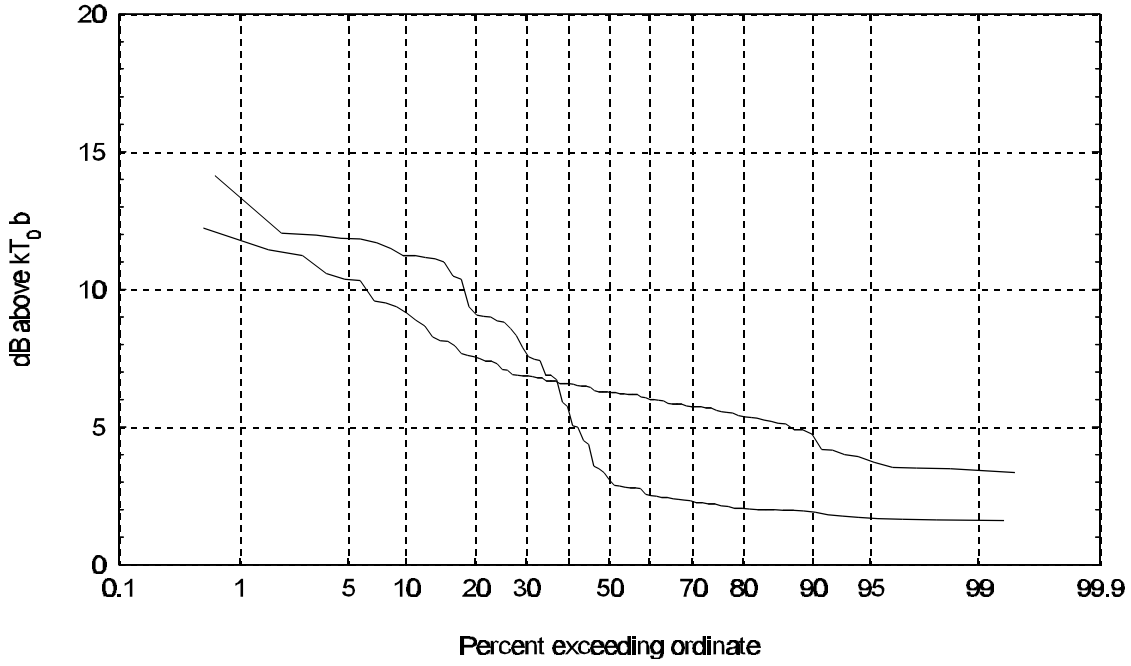

Figure 4.2 Cumulative distribution functions of the mean values for two residential locations.

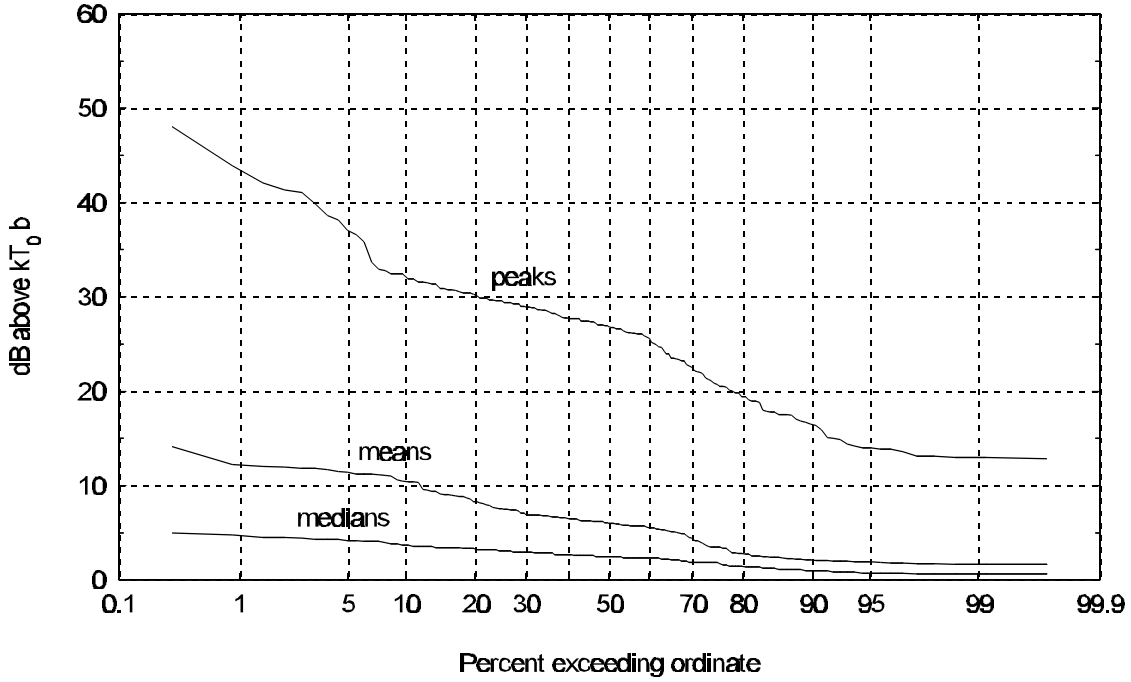

Figure 4.3 Cumulative distribution functions of the combined median, mean, and peak values of Lakewood, Colorado, and Boulder, Colorado, residential locations.

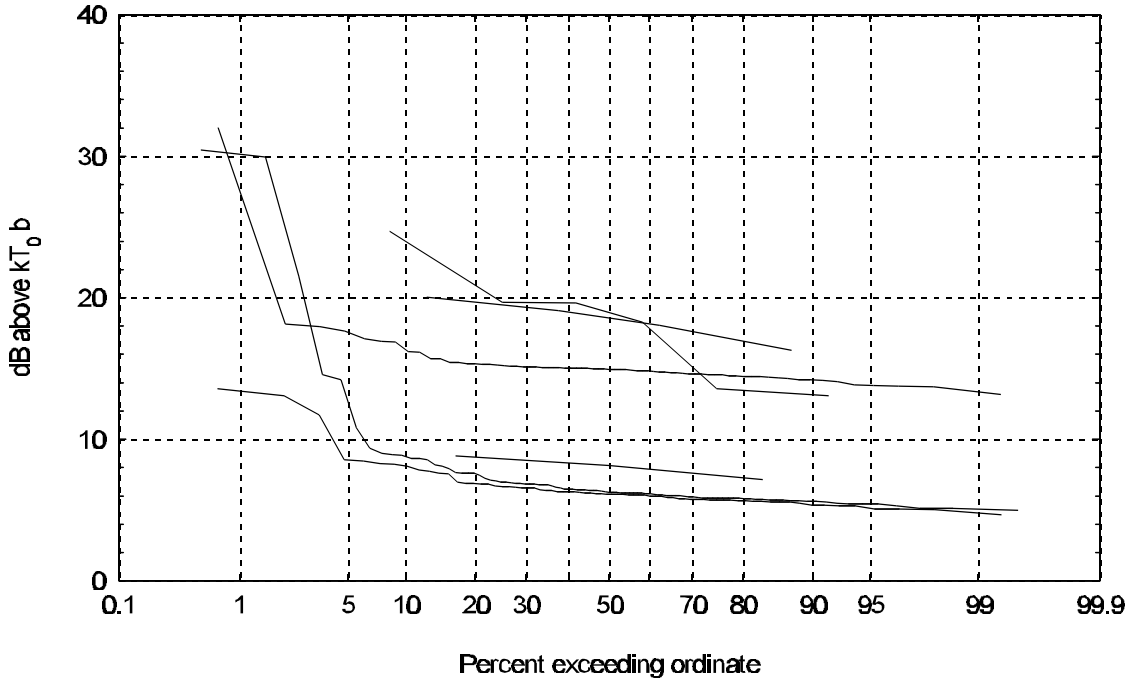

Figure 4.4 Cumulative distribution functions of the mean values for six business locations.

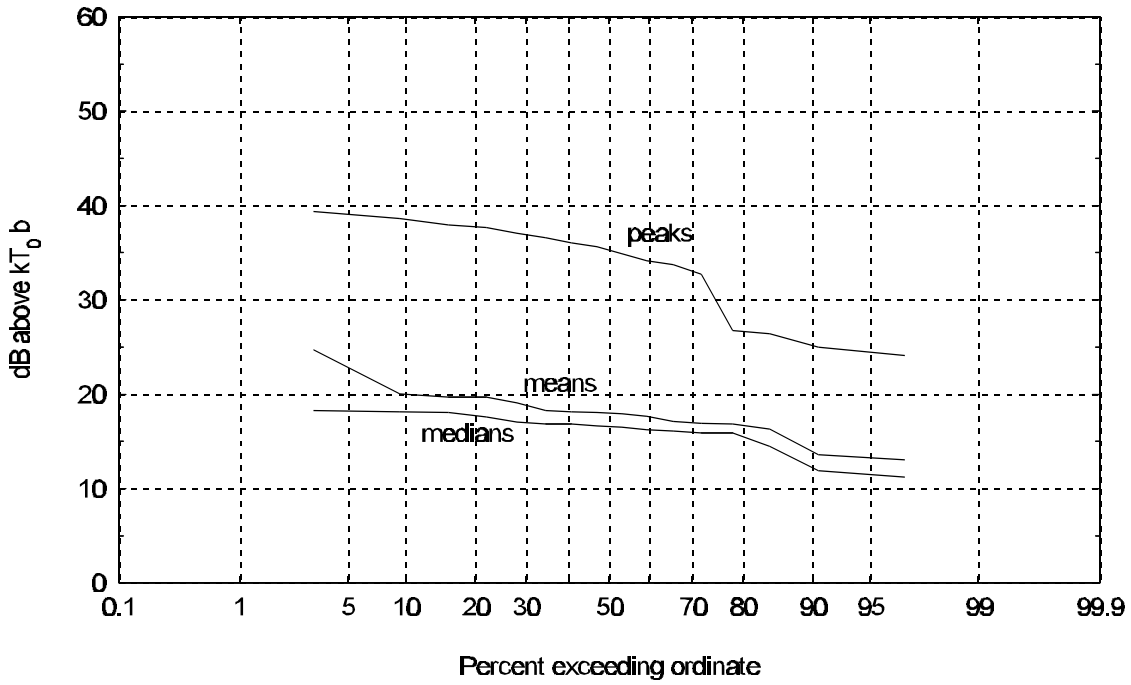

Figure 4.5 Cumulative distribution functions of combined median, mean, and peak values for three business locations.

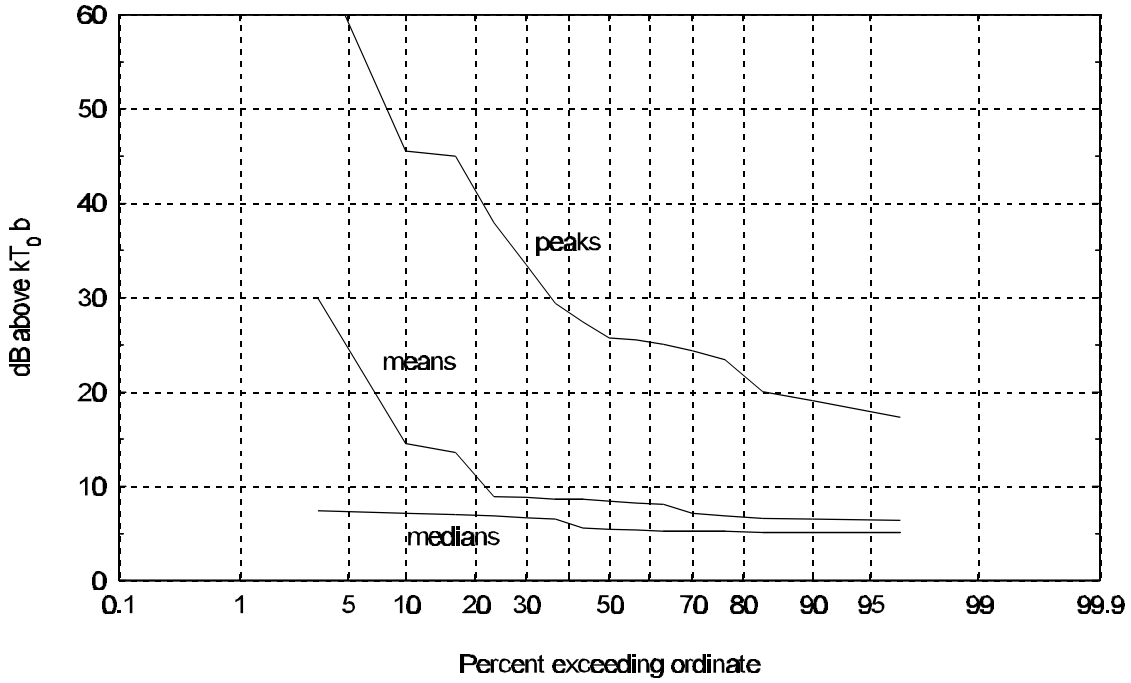

Figure 4.6 Cumulative distribution functions of combined median, mean, and peak values for three "light urban" locations.

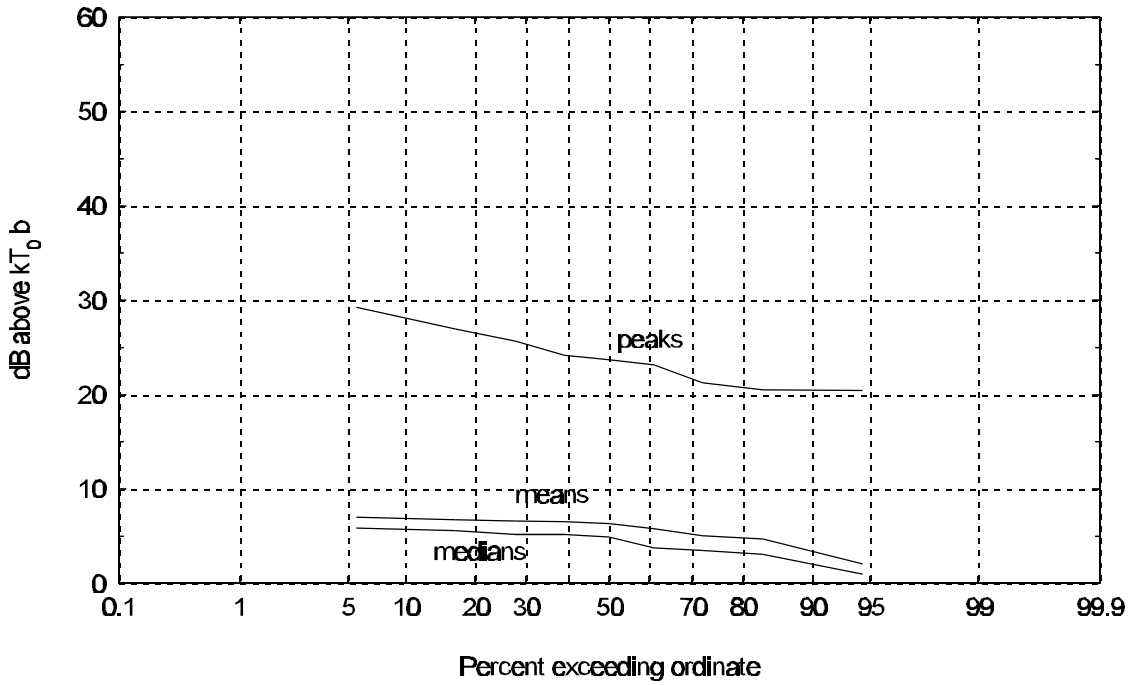

Figure 4.7 Cumulative distribution functions of combined median, mean, and peak values for four rural locations.

5. AMPLITUDE PROBABILITY DISTRIBUTION ANALYSIS

The effect of man-made noise, in the 136 to 138-MHz VHF meteorological satellite band, on radio links can be evaluated through simulation. In this section we describe how we used the noise power measurements to model man-made noise for radio link simulation.

5.1 Middleton Noise Model

To simulate man-made noise, it is desirable to first model the noise with analytical representations of the APD using as few statistical parameters as possible (e.g., moments and various measures of "impulsiveness"). To this end, Middleton [15-18] has published a detailed analysis of statistical-physical models of man-made and natural radio noise. This work is lengthy and detailed, consisting of four parts published over a period of more than 4 years.

Middleton's analysis of non-Gaussian noise is based on the assumption that the noise sources are Poisson distributed in space and time and that "source waveforms" can have random amplitudes, durations, and frequencies. In this work, noise is divided into classes based on the interaction of the time-varying noise voltage and the receiver. Class A noise, composed of Gaussian noise and random pulses, is defined as having a bandwidth that is significantly smaller than the receiver filter of interest (the final IF filter for our purposes). With this assumption, the APD of received instantaneous power w is:

$$A_1(w) \approx e^{-\gamma T} \sum_{m=0}^{\infty} \frac{(\gamma T)^m}{m!} e^{-w/(2\sigma^2 + m\rho^2)} \tag{5.1}$$

where (is the mean pulse arrival rate, T is the mean pulse duration, D^2 is the average pulse power, and 2F^2 is the average Gaussian noise power. In this equation the APD depends on the "impulse index" (T and not explicitly on (or T. Thus, only three parameters are required to model the ADP of Class A noise. Furthermore, the average received power is roughly proportional to (T; hence, the IF filter should not affect the shape of the APD as long as its bandwidth is large when compared to the random pulse bandwidth.

Class B noise is defined as having a bandwidth that is larger than the receiver filter of interest. The resultant APD as calculated by Middleton consists of three components: a Gaussian component, a rare event component, and an intermediate event component. The Gaussian and rare event components have the same functional form as Equation (5.1). The intermediate component is much more complicated and includes an infinite series of confluent hypergeometric functions (M):

$$A_2(w) = w \sum_{n=0}^{\infty} \frac{(-1)^n A_\beta^{\,n}}{n!} \Gamma\left(1 + \frac{\beta n}{2}\right) M\left(1 + \frac{\beta n}{2}, 2, -w\right) \tag{5.2}$$

where $A_\$$ is an "intermediate event impulse index", and $ is known as a "spatial density-propagation parameter" with the restriction $0 \# \$ < 2$. In addition to the three parameters required for A_1 and the

two parameters required for A_2, another parameter specifying the intersection point for the two functions must be used.

Clearly, the implementation of Equation (5.2) in practical simulations is likely to be onerous. In addition, the determination and implementation of the required six parameters appears to be quite tedious and as noted by Hagn [19], practical parameter estimation techniques deserve considerable additional attention.

Our data represent the noise statistics after the final IF filter in the measurement system. Since the actual receiver bandwidth may differ from the measurement system, it is desirable to simulate the noise process prior to the final IF filter. Determining the parameters that fit Equations (5.1) and (5.2) to our data does not achieve this end. We are able, however, to use these results as a guide in developing noise simulation models from our measurements as described below.

5.2 Simplified Noise Model

As indicated above, we were interested in developing a complex baseband, time series representation of the noise process prior to the final IF filter of our measurement system. Following Middleton, we assumed that as observed by the receiver, Class A and Class B noise have a non-Gaussian component with a randomly distributed time of arrival and a Gaussian component that is always present. The Gaussian component is modeled as

$$g_k e^{j\theta_k} \tag{5.3}$$

where g_k is the Rayleigh-distributed amplitude, θ_k is the uniformly distributed phase, and k is the time index.

The non-Gaussian pulse time of arrival was assumed to be Poisson distributed with pulse arrival rate γ. The probability that one pulse will arrive in t seconds is γt, therefore, the presence of a pulse is determined by

$$\chi_k = \begin{cases} 1 & \textit{with probability } \gamma \Delta t \\ 0 & \textit{with probability } 1 - \gamma \Delta t \end{cases}. \tag{5.4}$$

Representations of pulse duration and pulse amplitude differed between Class A and Class B noise. Prior to receiver filtering, the Class A noise was represented by rectangular pulses, p_k , whose duration corresponded to a bandwidth less than the receiver filter bandwidth. In contrast, prior to receiver filtering, the Class B noise was represented by pulses whose bandwidth exceeded the receiver filter bandwidth.

Class A noise pulse amplitude was characterized by a sudden "step" at low APD exceedence probabilities when plotted on Rayleigh paper. This suggested that a pulse or group of pulses with a constant pulse amplitude was present. Class B noise was characterized by a distribution of amplitudes at low APD exceedence probabilities indicating that a group of pulses with variable pulse

amplitudes was present. When $w >> 1$, the asymptotic expansion of the confluent hypergeometric function in Equation (5.2) yields [20]:

$$A_2(w) \approx \frac{1}{\pi}\sum_{n=0}^{\infty} \frac{(-1)^n}{n!} A_\beta^{\,n}\, \Gamma^2(\beta n)\, \beta n \sin(\pi \beta n)\, w^{-\beta n} \quad . \tag{5.5}$$

Setting $ << 1 and $A_\$ << 1$, so that only the first few terms of the series are important, A_2 can be approximated using a Weibull APD [21,22]:

$$A_2(w) \approx e^{(-w/w_{ow})^{1/\alpha}} \tag{5.6}$$

where w_{ow} and " are the Weibull parameters and

$$\xi\ \{w\}\ =\ w_{ow}\ \Gamma\ (\alpha + 1). \tag{5.7}$$

In summary, our complete simplified Class A noise model is

$$v_k = B e^{j\Phi}\ \sum_{l=1}^{\infty} p_l\, \chi_{k-l}\ +\ g_k\, e^{j\theta_k} \tag{5.8}$$

where B and N are the pulse amplitude and phase. The complete simplified Class B noise model is

$$v_k = (b_k \chi_k + g_k)\, e^{j\theta_k} \quad , \tag{5.9}$$

where b_k is the Weibull distributed amplitude of the non-Gaussian noise component.

The Weibull distributed amplitude is generated by

$$b_k = \sqrt{w_{ow}}(-\log_e u_k)^{\alpha/2} \quad , \tag{5.10}$$

where u_k is a uniformly distributed random variable with a range from 0 to 1. In a similar way the Rayleigh distributed amplitude was generated by

$$b_k = \sqrt{w_{og}}(-\log_e u_k)^{1/2} \quad , \tag{5.11}$$

where w_{og} is the mean Gaussian power.

A number of our measurements show that in addition to impulsive noise, there were "constant" noise sources with bandwidths narrower than our IF filter. The constant noise may originate from periodic, pulsed emissions from nearby electrical and electronic equipment. The constant noise component was characterized by a decrease in the slope of the straight line at high APD exceedence probabilities. These noise sources were modeled by adding a constant to the Gaussian noise component

$$z_k = g_k e^{j\theta_k} + c \tag{5.12}$$

where c is a constant. The amplitude of the resulting variate is Nakagami-Rice distributed

$$p(|z|) = 2|z|(1+K)\exp(-|z|^2[1+K]-K)\, I_0(2|z|\sqrt{K[1+K]}) \tag{5.13}$$

where

$$K = \frac{|E\{z\}|^2}{E\{|z-E\{z\}|^2\}} = \frac{|c|^2}{w_{og}} \tag{5.14}$$

is the ratio of constant noise-power to Gaussian noise-power. When plotted on Rayleigh paper, the Nakagami-Rice cumulative distribution function is approximately a straight line with a slope that depends on the K (see e.g., Figure 2.6).

5.3 Extraction of Noise Model Parameters from Measurements

The APD's used for simulation were composed of several measured histograms from each environment. Combining histograms was necessary to increase the accuracy of the low exceedence probability estimates. For most of our measurements w_{og} was estimated readily from the APD's 37th percentile amplitude. For Class A noise two additional parameters were extracted from the APD: (T and B. For Class B noise, three additional parameters were required for each Poisson/Weibull process: (T, ", and w_{ow}.

The product (T is estimated from the APD exceedence probability associated with a departure from a Rayleigh distribution. The parameter (was calculated from the product (T after T was measured or estimated. For Class A noise we assumed T was much greater than the receiver filter time constant, therefore, the T before and after the receiver filter was the same. For Class B noise, prior to filtering, the pulse was assumed to be an impulse. After filtering, the pulse duration was estimated to be the duration of a unit amplitude, rectangular pulse with approximately the same area as the filter impulse response.

The constant amplitude of Class A noise was read directly from the amplitude of the low exceedence probabilities of the APD. The Weibull distribution parameters " and w_{ow} of Class B noise are ideally estimated from the slope and amplitude of the lower exceedence probability events whose event spacing is much greater than the filter time constant. In practice, for many of the Class B

APD's, there was not sufficient data to measure ". In these cases, " was adjusted empirically to provide the best fit.

Using the estimated parameters, the simulated time series was passed through a digital implementation of our noise measurement receiver final IF filter, and the resultant APD was compared with the measured APD. It was found that, except for w_{og}, several iterations were required to determine the optimum parameter values.

5.4 Simulation Results

For our analysis, we selected measurements that covered a variety of man-made noise environments. These APD's represent typical examples of first-order statistics for a particular measurement location or environment. From the representative noise measurements in Section 3 only the rural environment and computer APD's have been excluded. The rural environment was excluded because it was the quietest environment. The computer APD was excluded because it was similar to the Nakagami-Rice APD found in the office park. As indicated above, these Class A and Class B noise parameters characterize noise before the final IF filter of the measurement system. The simulated APD's shown in Figures 5.1 through 5.18 were filtered by a six-pole Chebychev filter with a 34-kHz noise equivalent bandwidth which approximated our noise measurement receiver filter. A 10-:s time increment was used. In the following discussion $w_o = E\{w\}$, $W_o = 10\log_{10}(w_o)$, $W_{og} = 10\log_{10}(w_{og})$ and $W_{ow} = 10\log_{10}(w_{ow})$.

Figure 5.1 shows an example of a Class A noise APD. For this simulation, the Class A noise pulse duration is 1.0 ms, pulse arrival rate is 0.3 pulses/second, and the pulse amplitude is 67.0 dB above kT_0b. Class B noise also is included in this simulation. The Class B noise parameters are " = 1.0, (= 30.0 pulses/second, and W_{og} = 7.3 dB, W_{ow} = 27.0 dB, W_o = 33.4 dB above $kT_0 b$. Class A noise with large amplitudes was observed at many of our measurement sites. The time between Class A noise events, however, was on the order of hours, and the duration of the events was less than 100 ms. Since our measurements indicated that Class A events are rare and of short duration, the remainder of our analysis focused on the simulation of the more common Class B noise.

In Table 2 we have tabulated the simulation parameters for Class B noise corresponding to several man-made noise locations and sources. Figures 5.2 through 5.16 show the comparison between the measured and simulated APDs for each entry in Table 2. Note that in some cases, two non-Gaussian noise components are required to obtain a suitable APD. This may be the case, for example, when both strong power line and automotive noise sources are present.

Figures 5.17 and 5.18 show Nakagami-Rice distributed APD's from the office park measurements. Electrical or electronics equipment with periodic, pulsed emissions may be a source of constant narrowband noise. The Class B and Nakagami-Rice parameters for Figure 5.17 are K = 3.0 dB, " = 2.0, (= 0.8 pulses/second, and W_{og} = 11.0 dB, W_{ow} = 32.0 dB, W_o = 14.5 dB above kT_0b. The Class B and Nakagami-Rice parameters for Figure 5.18 are K = 3.0 dB, " = 2.0, (= 10.0 pulses/second,

and W_{og} = 11.0 dB, W_{ow} = 32.5 dB, W_o = 14.7 dB above kT_0b. Figure 3.3b shows the median, mean, and peak power for this time and location.

5.5 Change of Simulation Time Increment

When performing Class B noise simulations, the average power of the non-Gaussian component depends on the time increment as follows:

$$<W_{ow}(dB/kT_o)> \;=\; W_{ow}(dB/kT_o) + 10\log_{10}(\gamma\,\Delta t)\;. \tag{5.15}$$

where Δt is the simulation time increment. The tacit assumption in our model is that prior to the final IF filter, Class B noise can be treated as a series of pulses having a duration less than Δt. The Δt for a particular receiver analysis would, of course, be based on the bandwidth of the receiver IF filter.

To determine W_{ow} for a different time increment the average powers of the non-Gaussian processes are equated at the two time increments, and therefore

$$W'_{ow}(dB/kT_o) = W_{ow}(dB/kT_o) + 10\log_{10}\left(\Delta t / \Delta t'\right) \tag{5.16}$$

where the prime denotes Δt and W_{ow} values at the new time increment.

Table 2 Simulation Parameters for Various Noise Environments

Related Figures	Location	Environment or Source	Date mm/dd/yy	Time hh:mm	(pulses/s	"	W_{ow} dB relative to kT_o*	W_{og} dB relative to kT_o	W_o dB relative to kT_o
5.2 3.1a	Lakewood, Colorado	Residential	11/10/96	12:00 a.m. 12:40 a.m.	220.0	0.5	31.0	4.6	6.9
5.3 3.1a	Lakewood, Colorado	Residential	11/10/96	3:30 p.m. 4:00 p.m.	220.0 2.0	0.5 0.5	23.0 62.0	5.1	15.0
5.4 3.1b	Lakewood, Colorado	Residential	11/11/96	12:16 p.m. 12:46 p.m.	1.5	3.0	43.0	4.6	5.6
5.5 3.2a	Boulder, Colorado	Residential	11/16/96	12:00 a.m. 12:30 a.m.	30.0	3.0	18.0	3.2	3.4
5.6 3.2b	Boulder, Colorado	Residential	11/17/96	9:00 a.m. 9:30 a.m.	1500.0 3.0	0.75 1.0	32.0 43.0	5.0	13.5
5.7 3.3a	Office park near highway	Light Urban	11/25/96	12:00 a.m. 1:00 a.m.	220.0 4.5	0.5 3.5	19.0 20.0	6.2	6.4
5.8 3.3a	Office Park near highway	Light Urban	11/25/96	12:00 p.m. 12:30 p.m.	30.0	3.5	19.0	8.3	8.6
5.9 3.3c	Office park near residential	Light Urban	11/30/96	12:00 a.m. 1:00 a.m.	2.0	5.0	25.0	5.7	5.8

Table 2, cont., Simulation Parameters for Various Noise Environments

Related Figures	Location	Environment or Source	Date mm/dd/yy	Time hh:mm	(pulses/s	"	W_{ow} dB relative to kT_o*	W_{og} dB relative to kT_o	W_o dB relative to kT_o
5.10 3.3c	Office park near residential	Business	11/30/96	1:00 p.m. 1:30 p.m.	25.0	4.0	22.0	6.6	7.2
5.11 3.4a	Downtown Boulder, Colorado	Business	11/20/96	1:00 p.m. 1:30 p.m.	150.0	2.5	30.0	18.0	18.5
5.12 3.4b	Downtown Denver, Colorado	Business	12/03/96	11:00 a.m. 11:30 a.m.	25.0	3.0	34.0	19.0	19.1
5.13 3.4b	Downtown Denver, Colorado	Business	12/03/96	11:20 a.m. 11:50 a.m.	60.0	2.5	35.0	19.0	19.4
5.14 3.6	Clear Creek Canyon, Colorado	Automotive	12/21/96	1:00 p.m. 1:30 p.m.	25.0	3.0	15.0	5.5	5.5
5.15 3.6	Clear Creek Canyon, Colorado	Automotive	12/21/96	2:00 p.m. 2:30 p.m.	15.0	6.0	16.0	5.3	6.3
5.16 3.7	Leyden, Colorado	Electrical Network	11/12/96	2:02 p.m.	495.0	0.5	46.0	5.0	22.6

* depends on the time increment of the simulation (see equation 5.15).

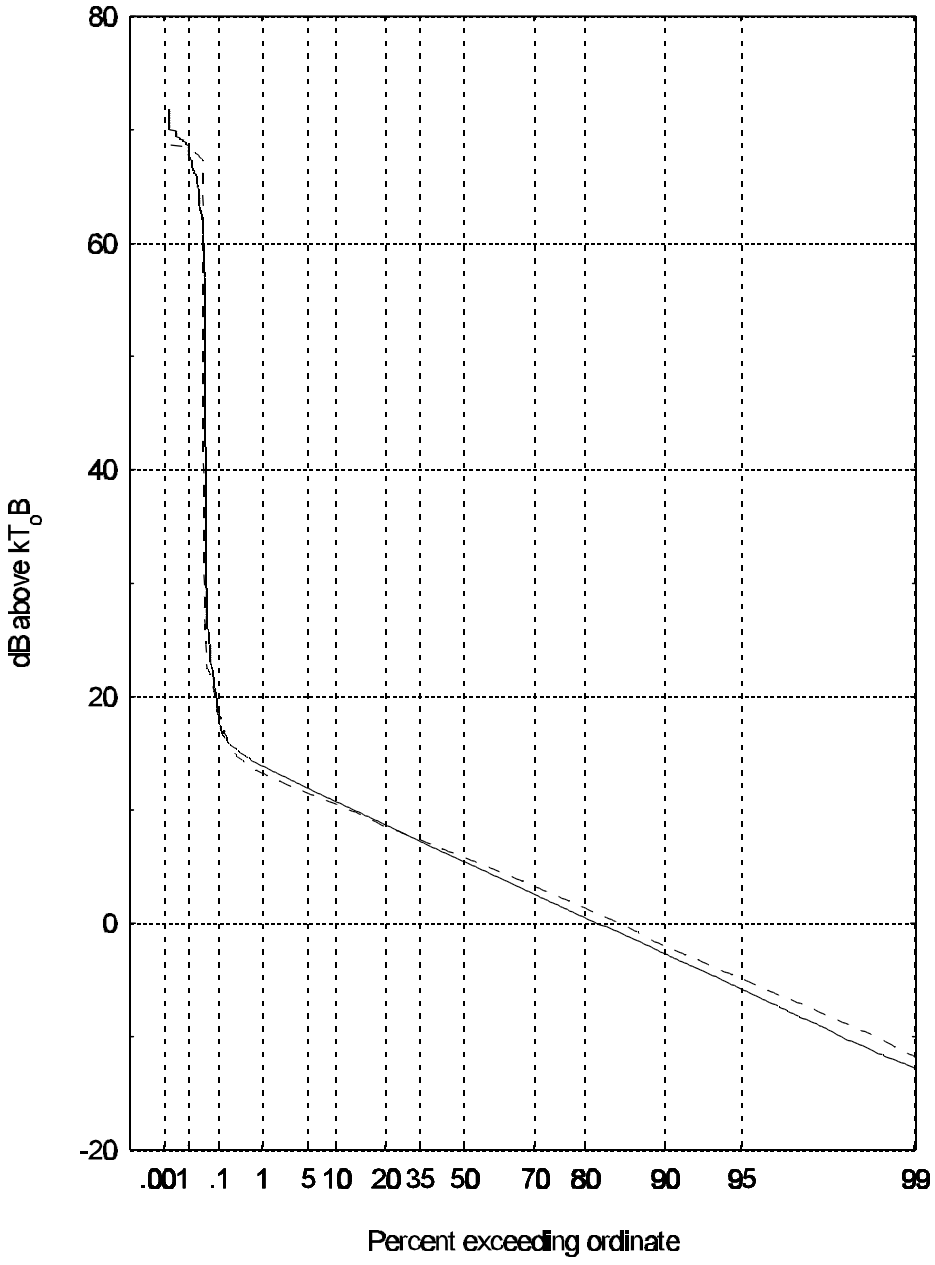

Figure 5.1 Class A noise from measurements at Plainview Open Space site near Boulder, Colorado, on November 7, 1996, at 3:11 p.m.

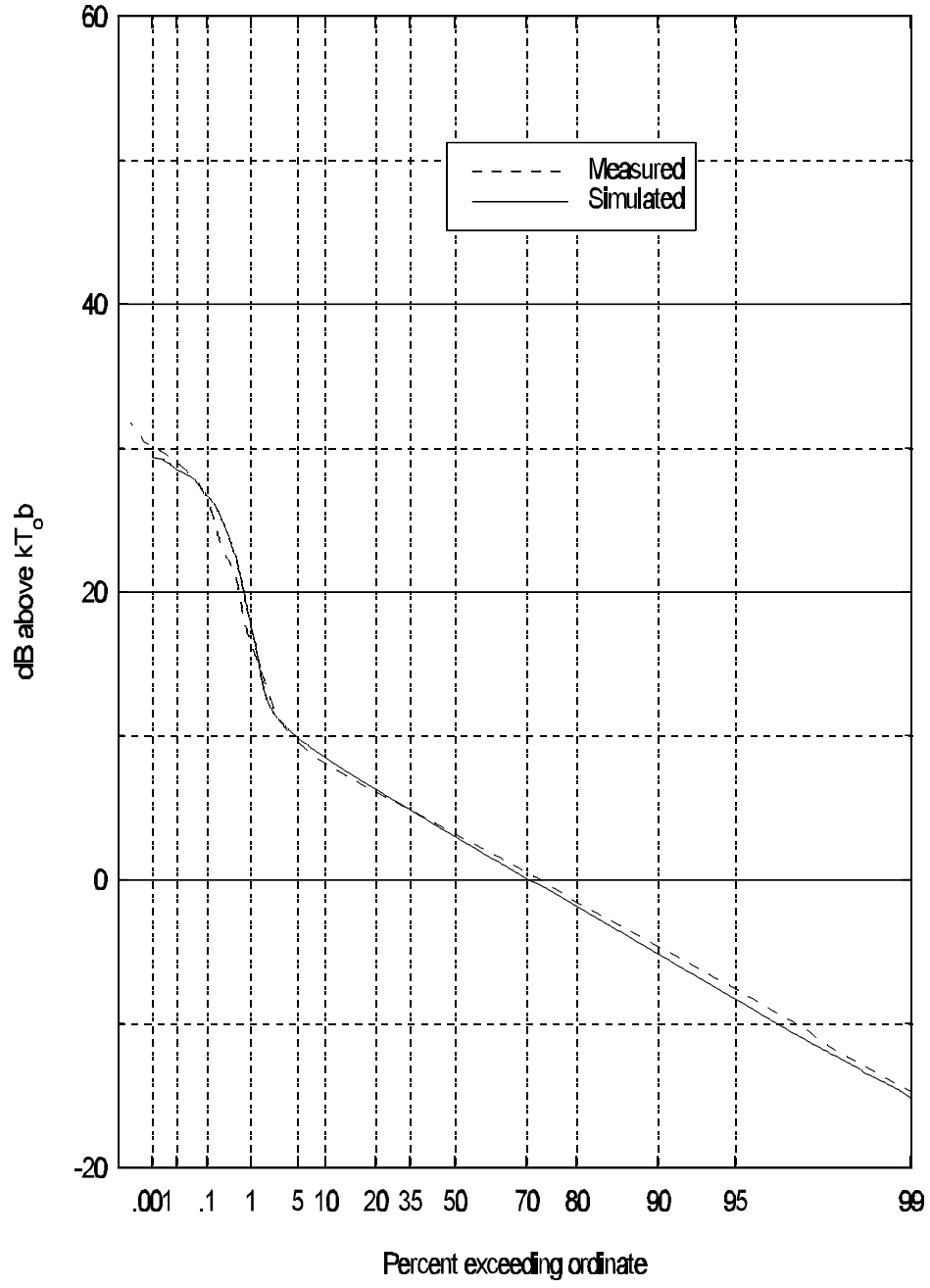

Figure 5.2 Class B noise from measurements at Lakewood, Colorado, residence on November 10, 1996, from 12:00 to 12:40 a.m.

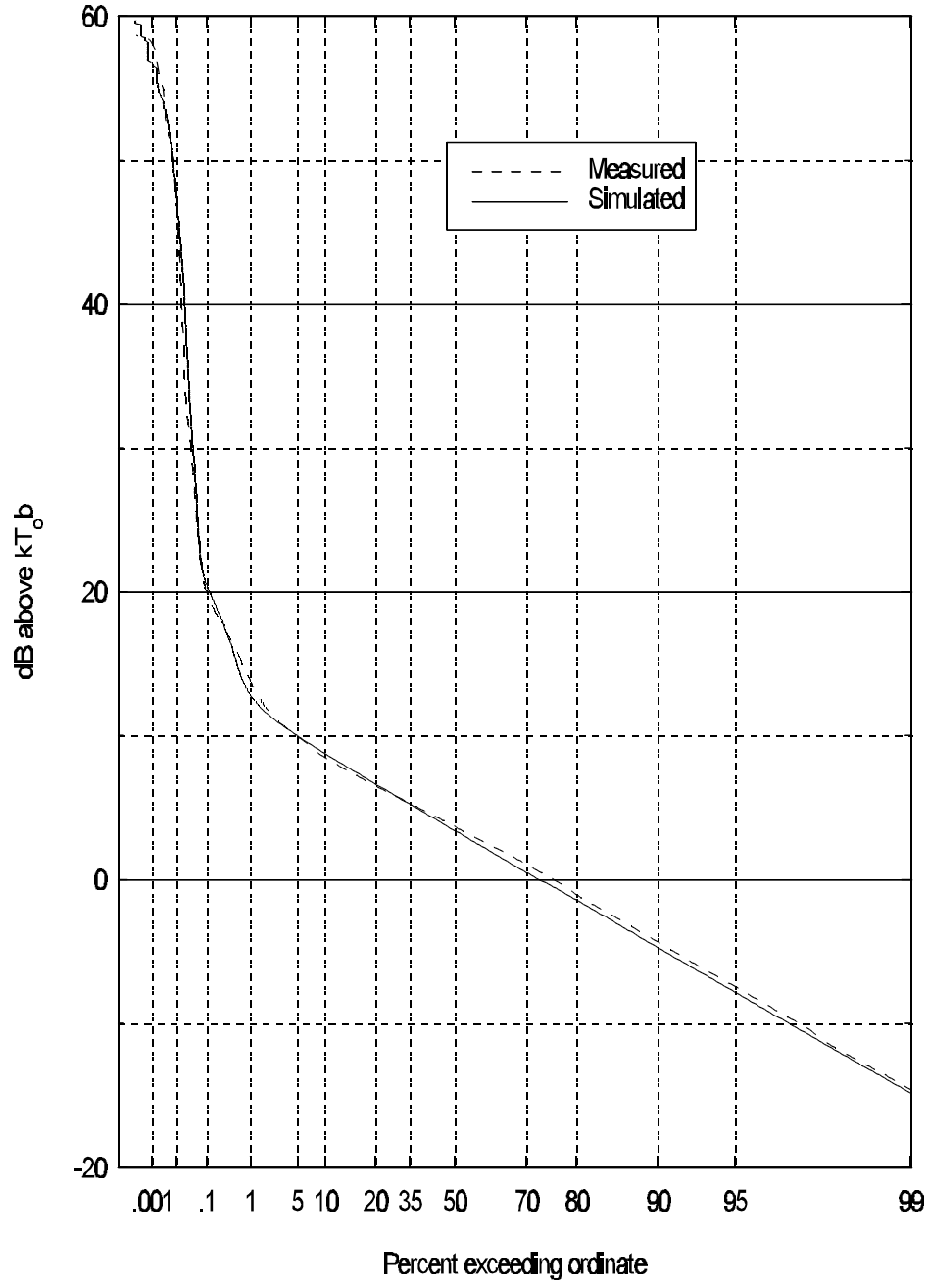

Figure 5.3 Class B noise from measurements at Lakewood, Colorado, residence on November 10, 1996, from 3:30 to 4:00 p.m.

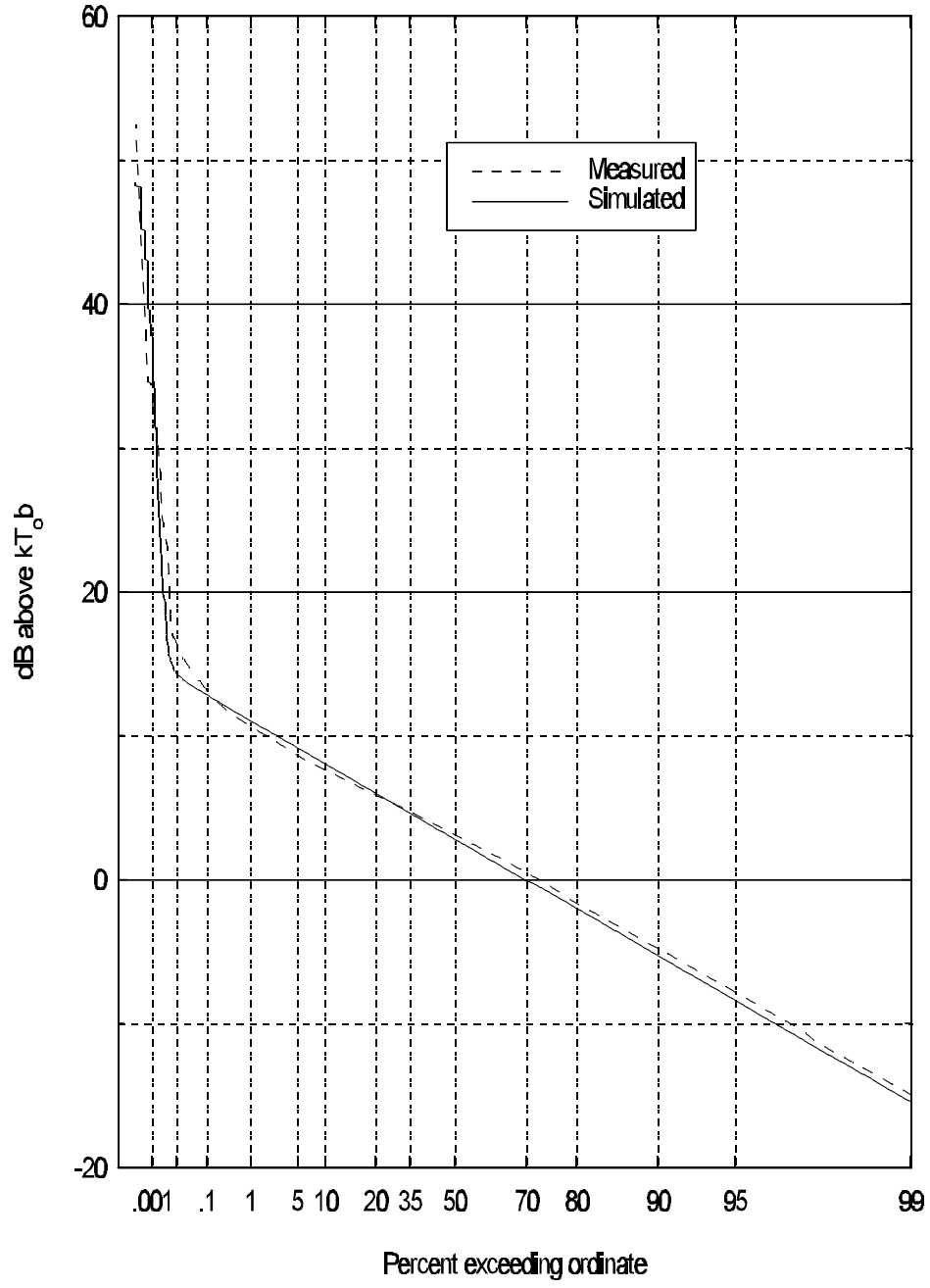

Figure 5.4 Class B noise from measurements at Lakewood, Colorado, residence on November 11, 1996, from 12:16 to 12:46 p.m.

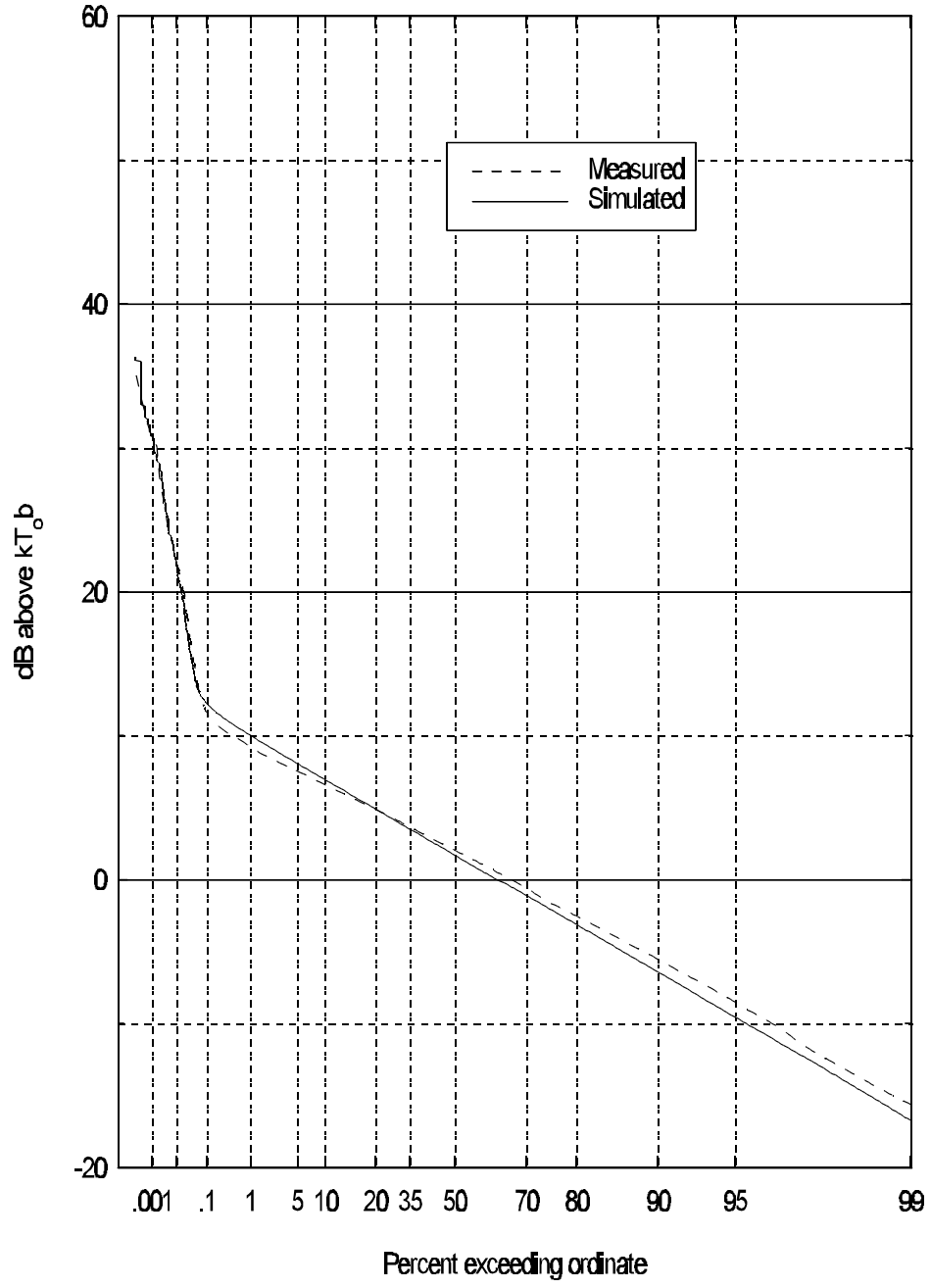

Figure 5.5 Class B noise from measurements at Boulder, Colorado, residence on November 16, 1996, from 12:00 to 12:30 a.m.

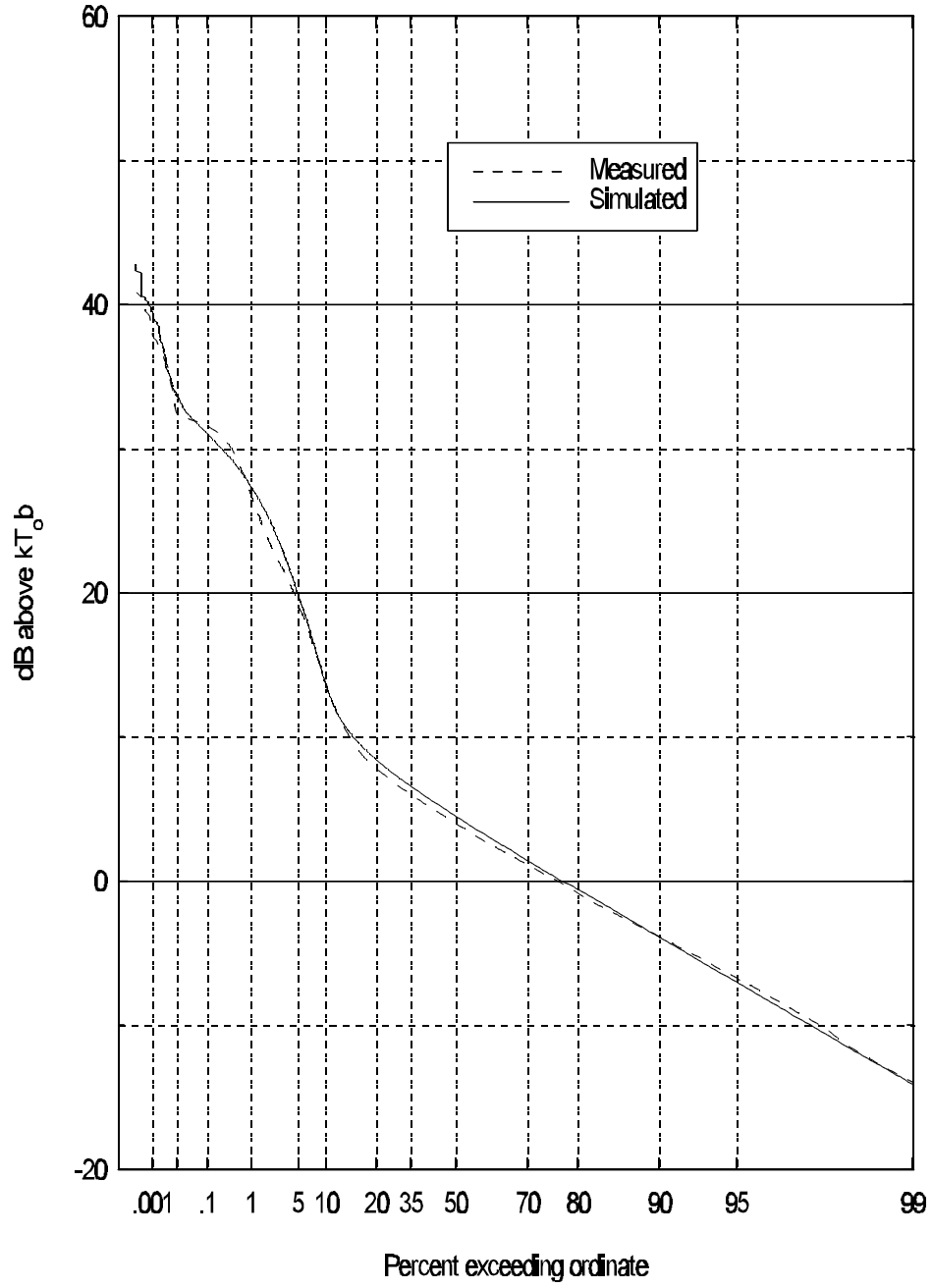

Figure 5.6 Class B noise from measurements at Boulder, Colorado, residence on November 17, 1996, from 9:00 to 9:30 a.m.

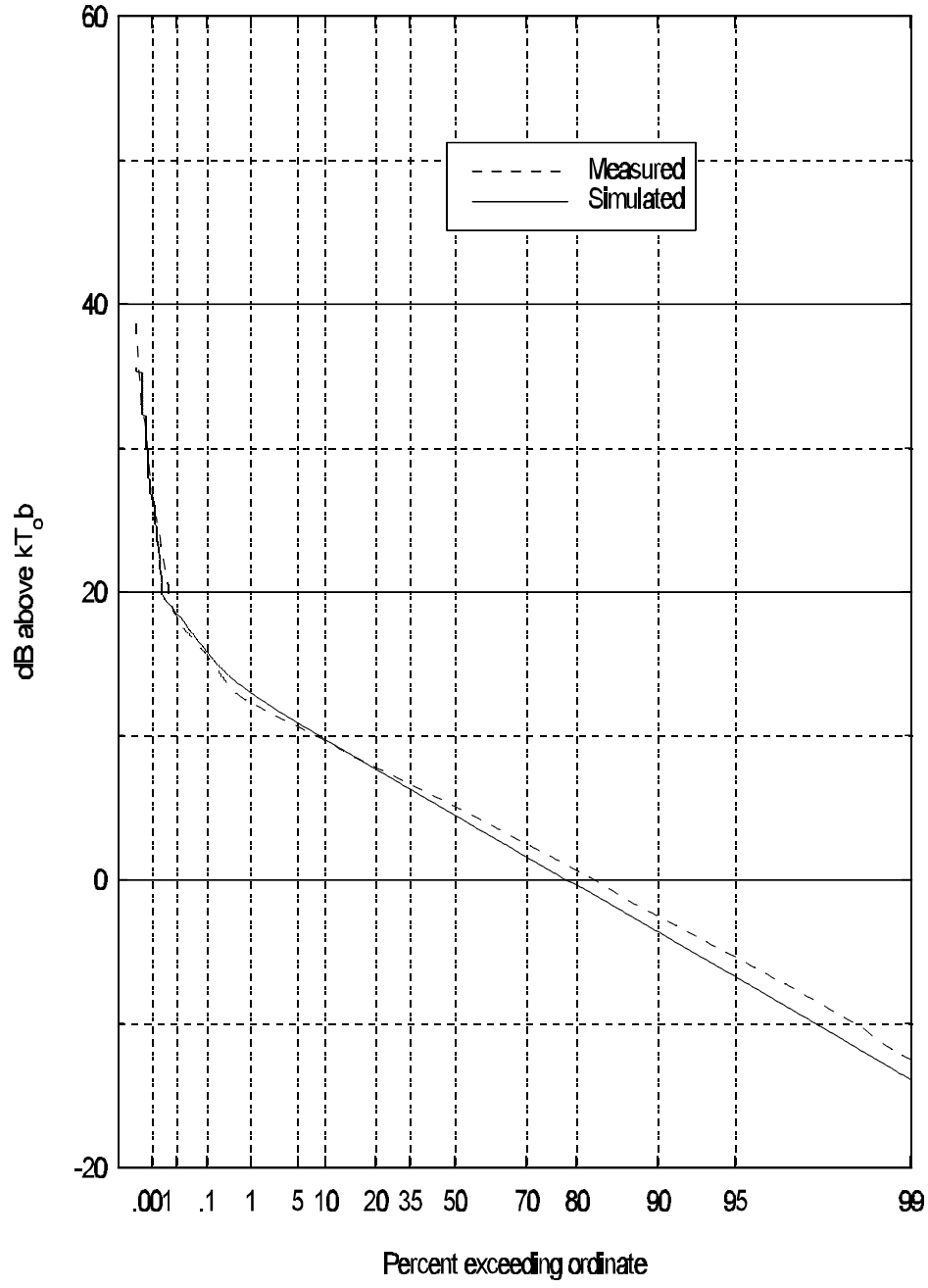

Figure 5.7 Class B noise from measurements in office park on November 25, 1996, from 12:00 to 1:00 a.m.

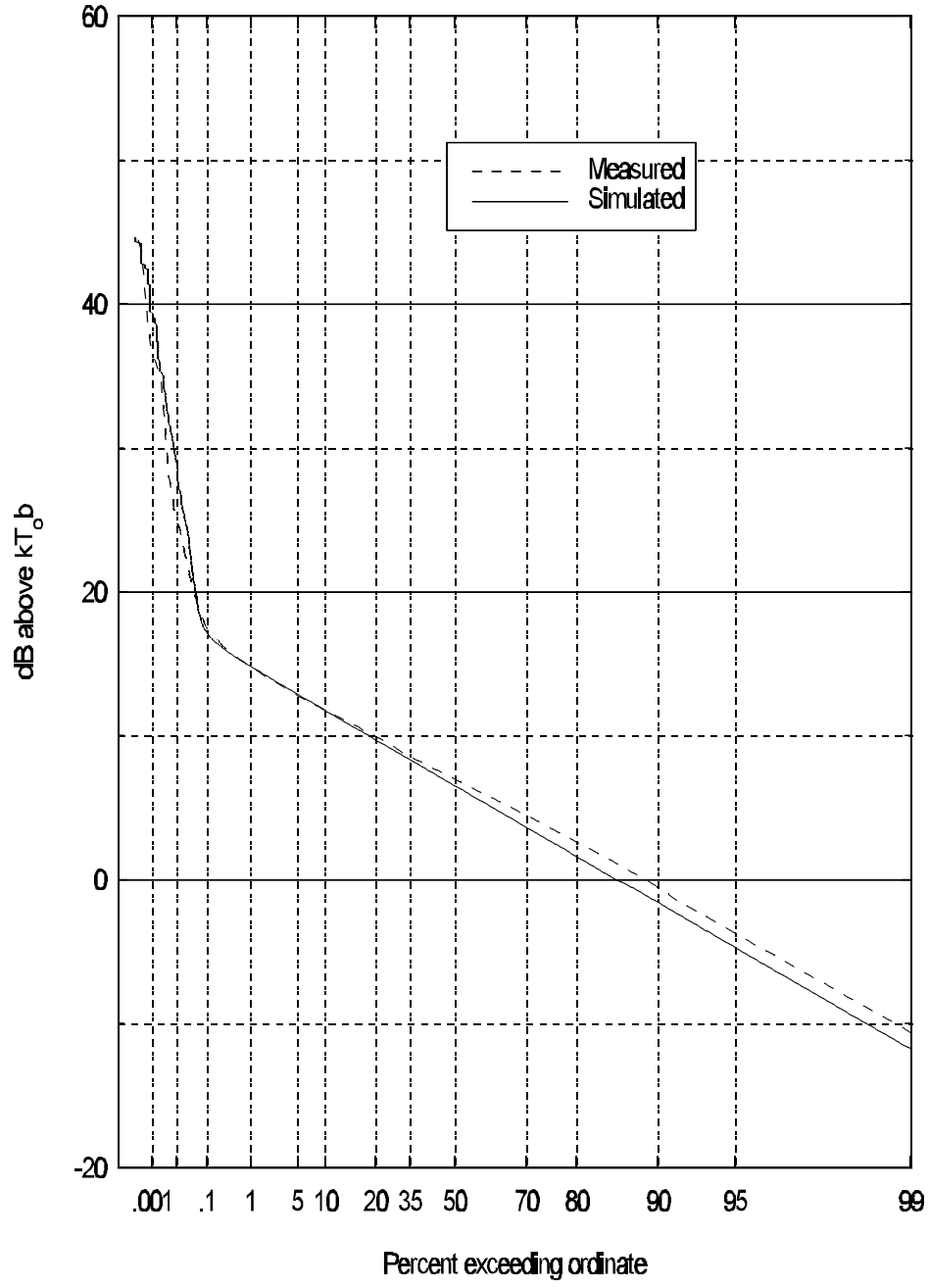

Figure 5.8 Class B noise from measurements in office park on November 25, 1996, from 12:00 to 12:30 p.m.

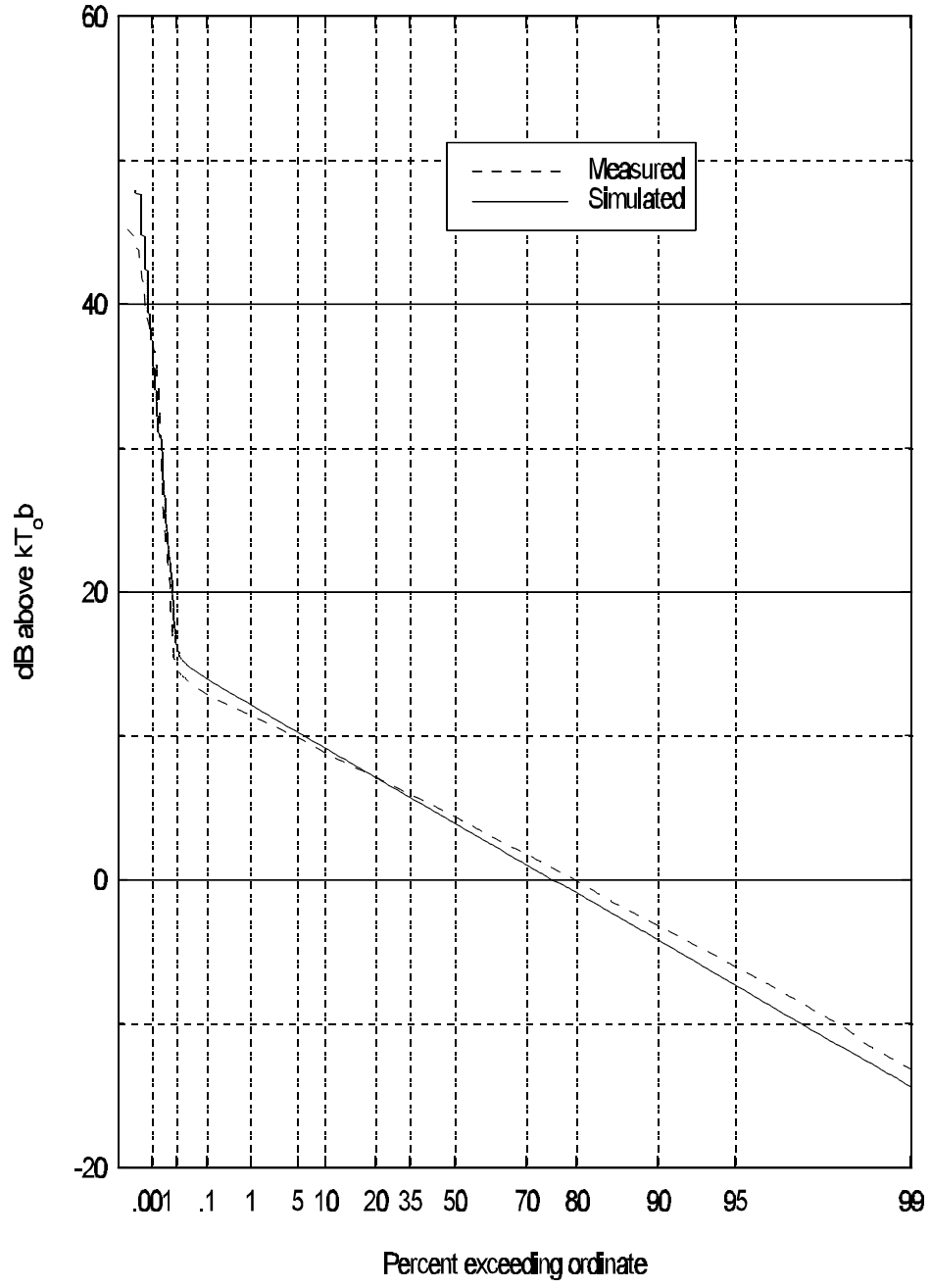

Figure 5.9 Class B noise from measurements in office park on November 30, 1996, from 12:00 to 1:00 a.m.

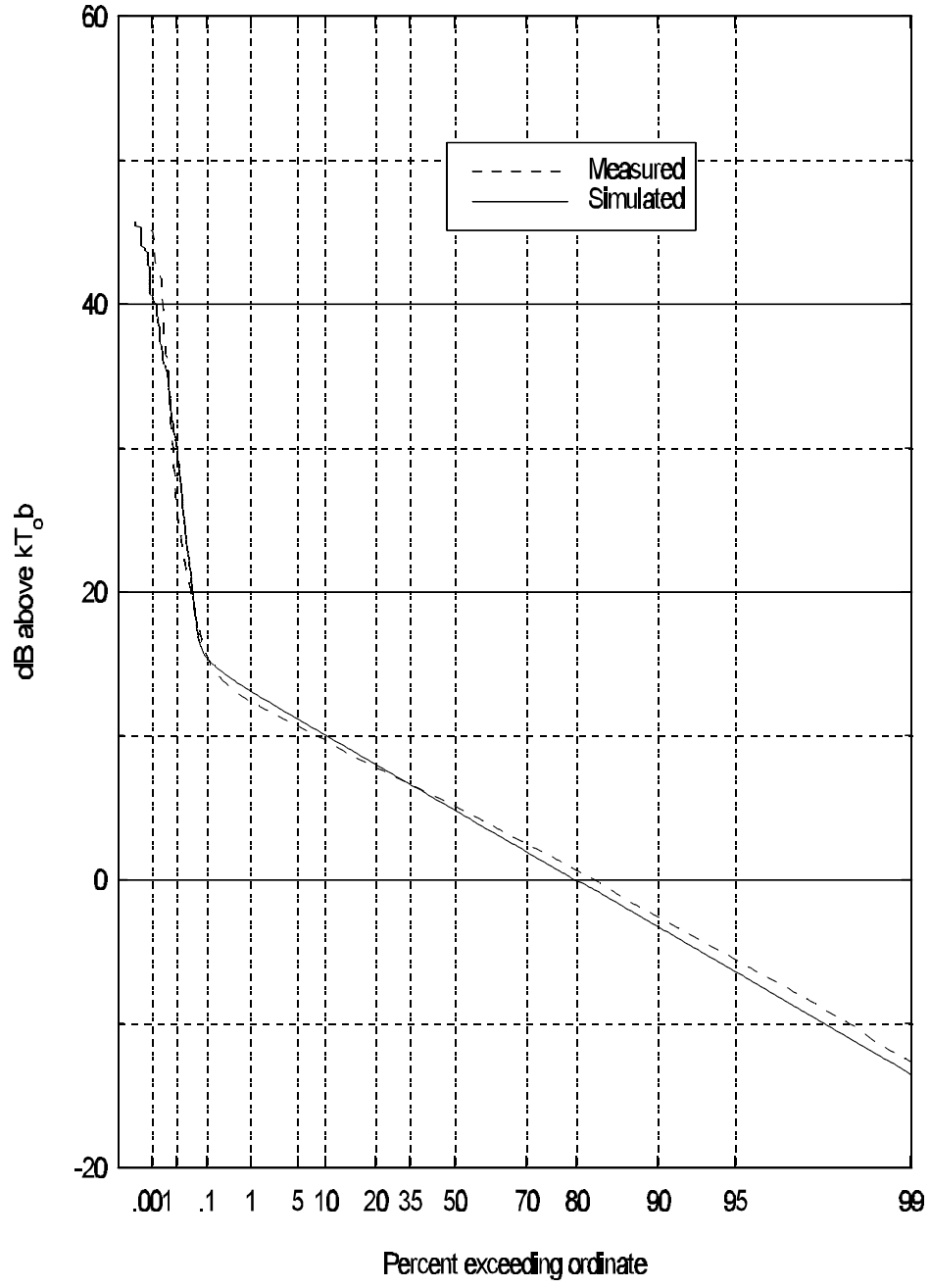

Figure 5.10 Class B noise from measurements in office park on November 30, 1996, from 1:00 to 1:30 p.m.

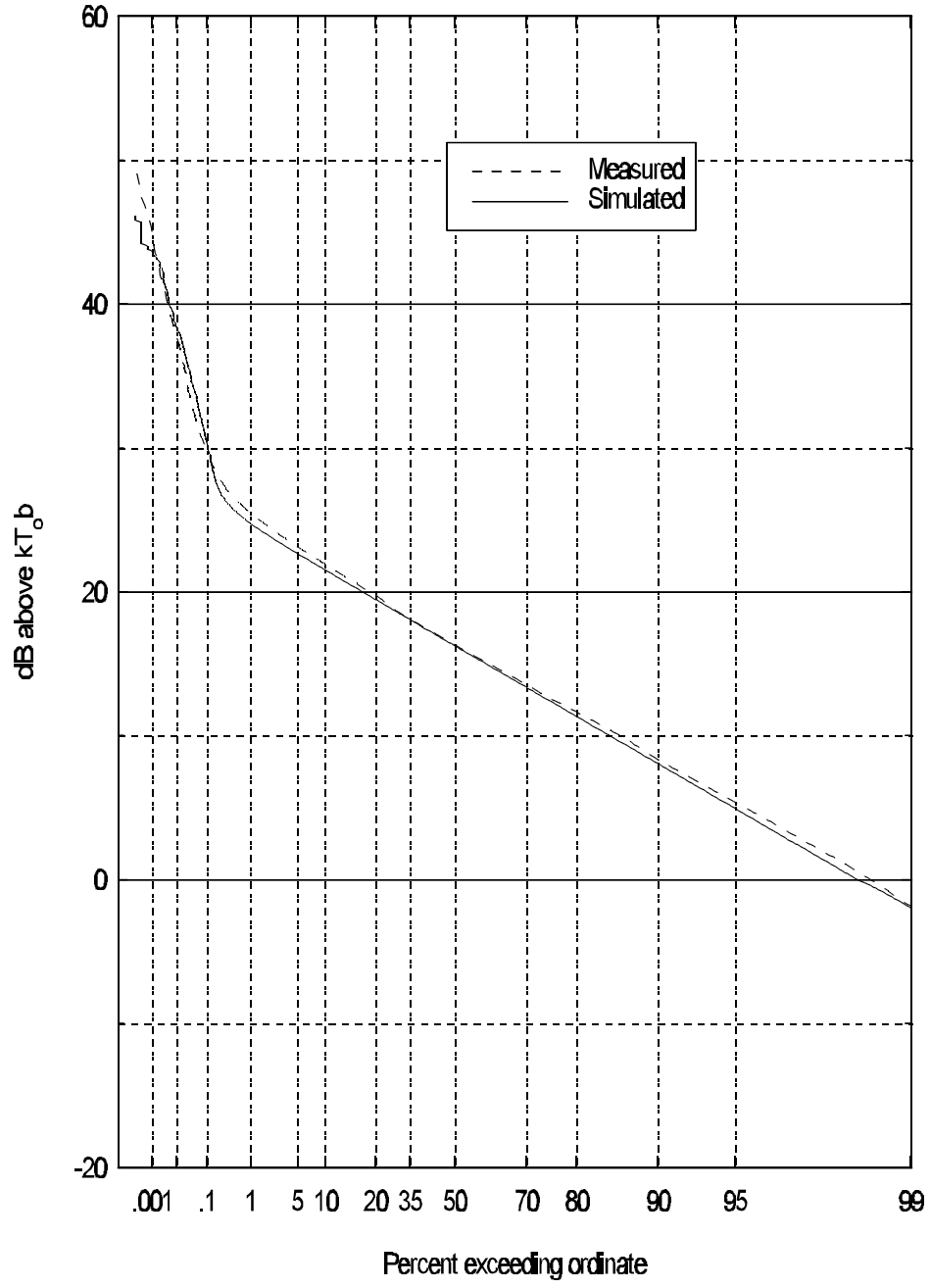

Figure 5.11 Class B noise from measurements in downtown Boulder on November 20, 1996, from 1:00 to 1:30 p.m.

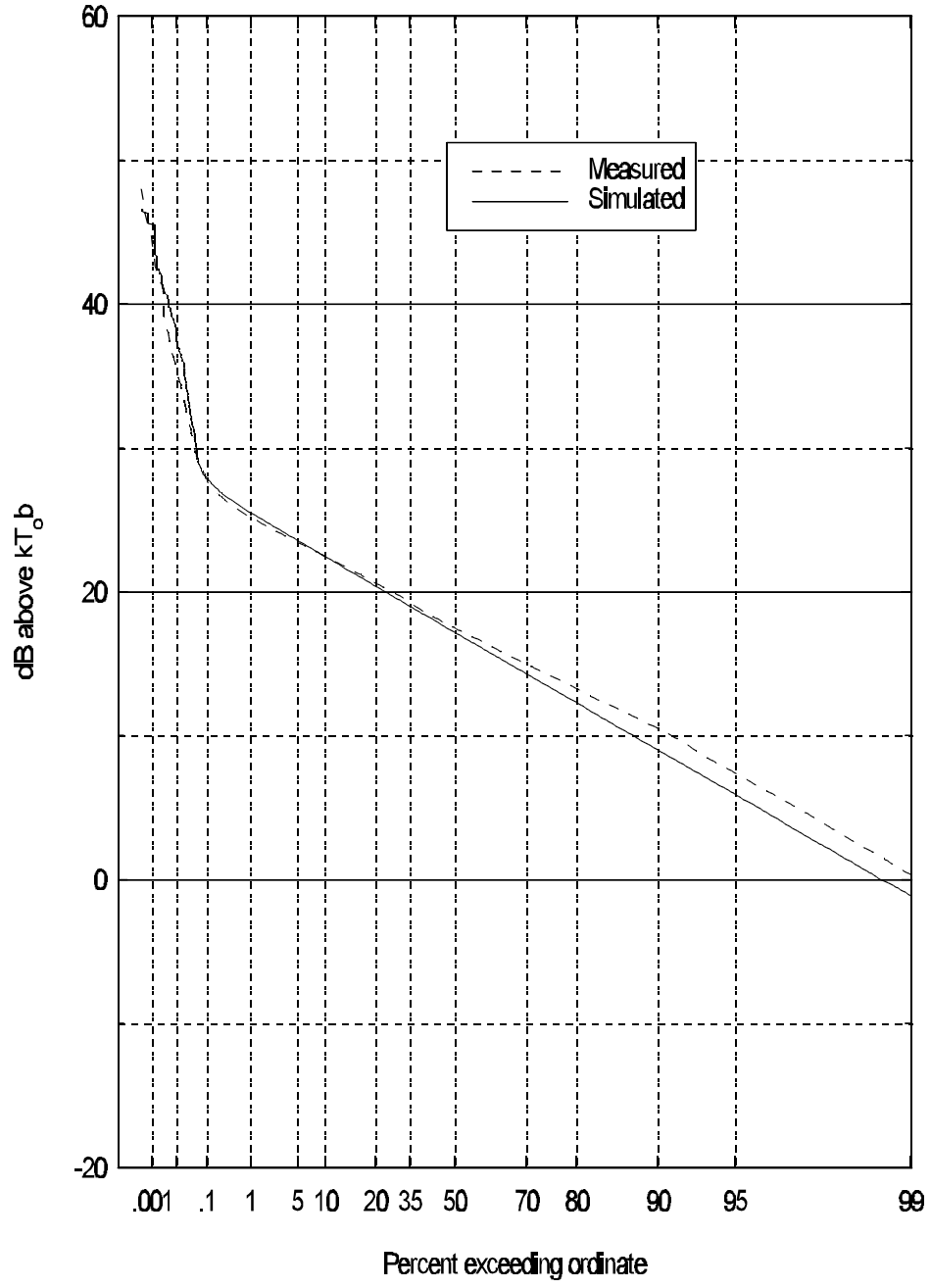

Figure 5.12 Class B noise from measurements in downtown Denver on December 3, 1996, from 11:00 to 11:30 a.m.

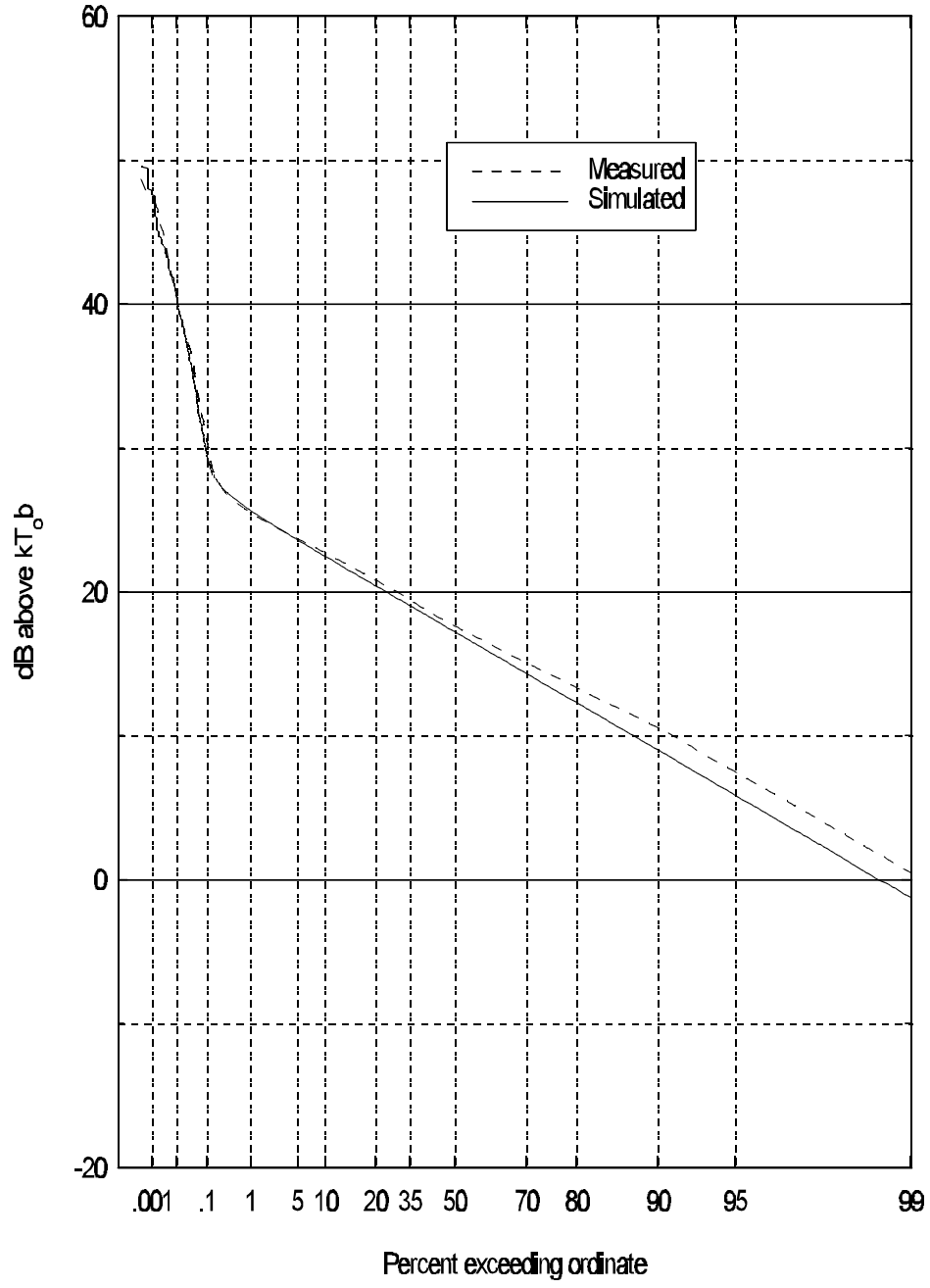

Figure 5.13 Class B noise from measurements in downtown Denver on December 3, 1996, from 11:20 to 11:50 a.m.

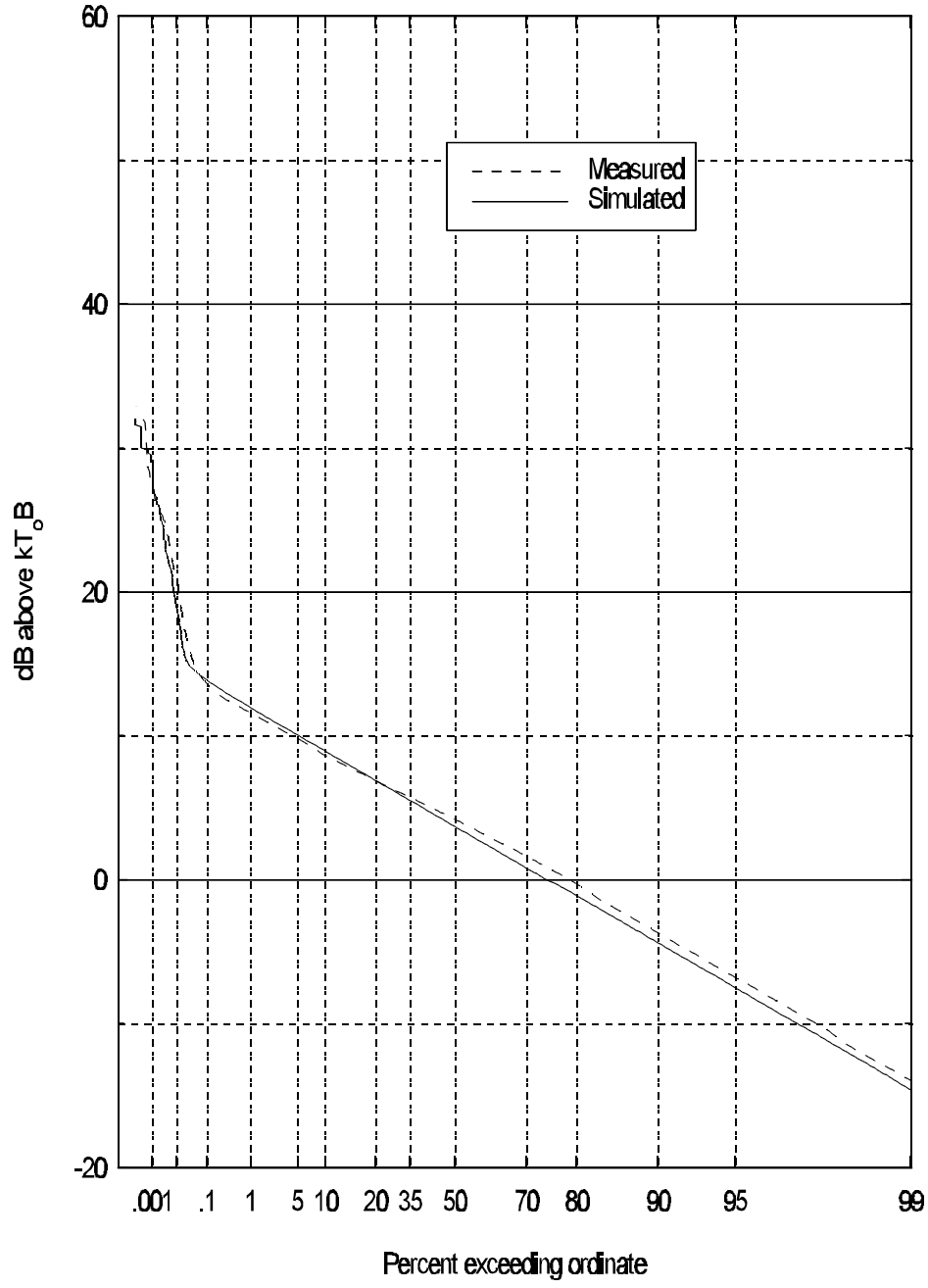

Figure 5.14 Class B noise from automobiles measured in Clear Creek Canyon, Colorado, on December 21, 1996, from 1:00 to 1:30 p.m.

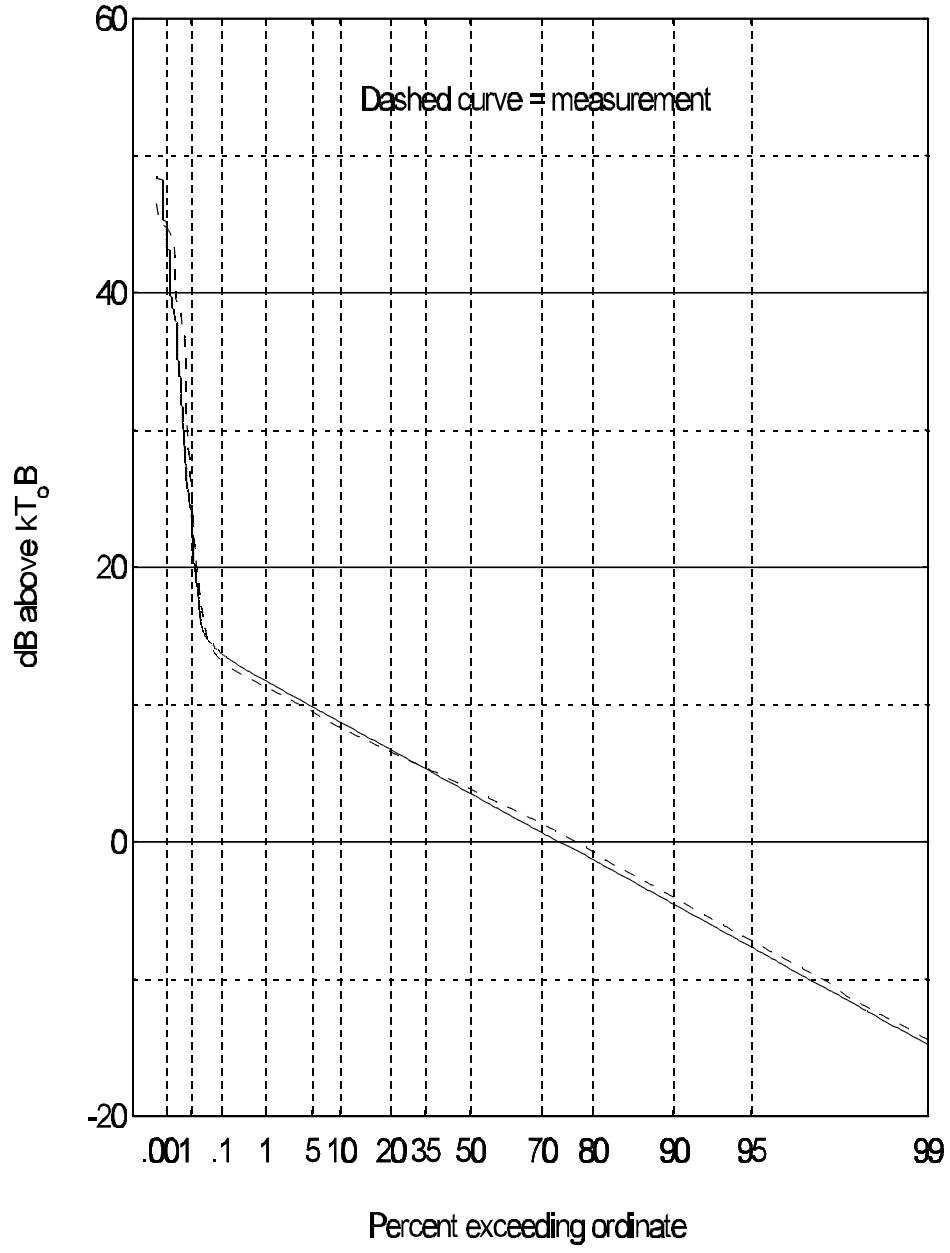

Figure 5.15 Class B noise from automobiles measured in Clear Creek Canyon, Colorado, on December 21, 1996, from 2:00 to 2:30 p.m.

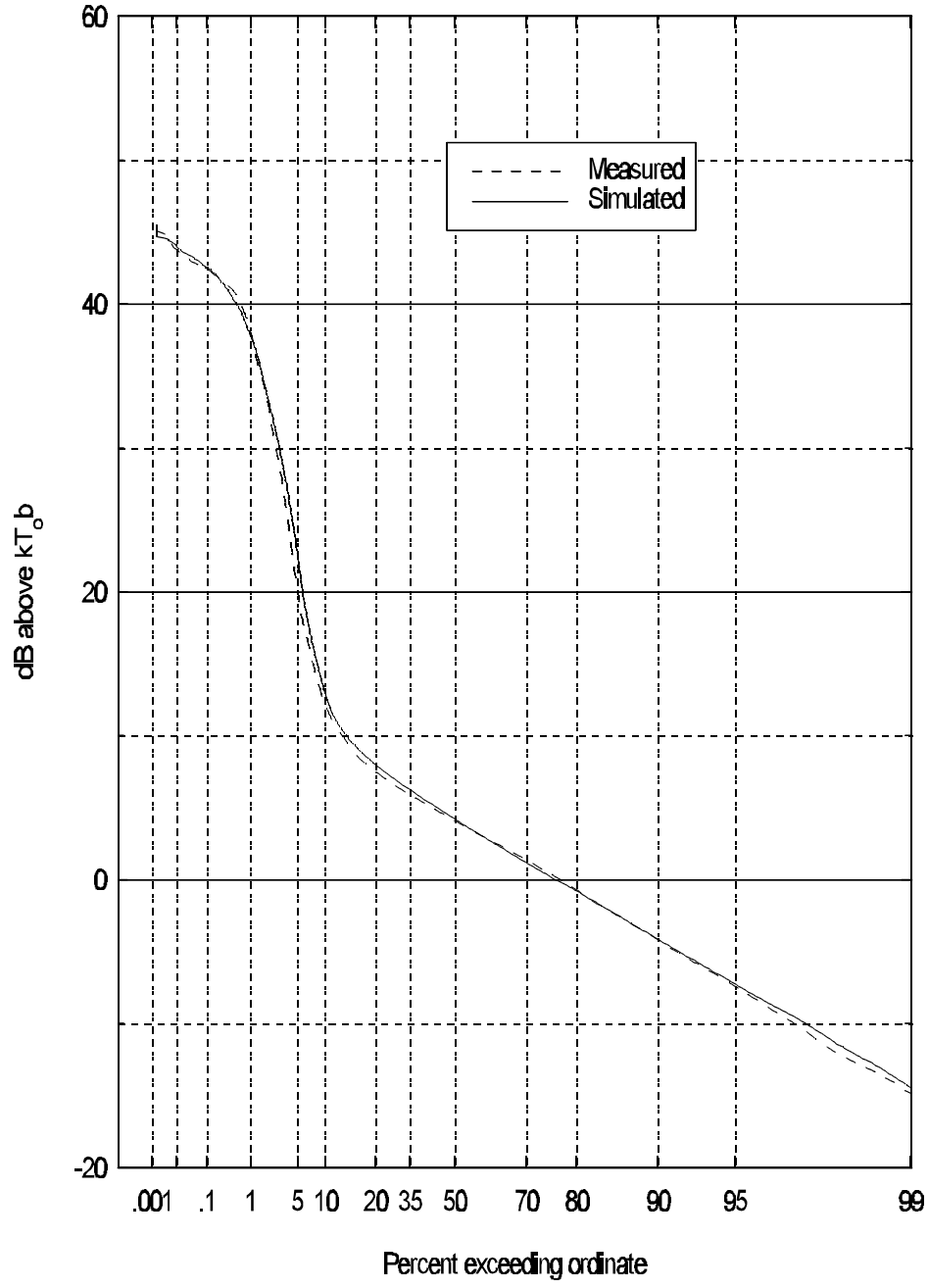

Figure 5.16 Class B noise from electrical network measured near Leyden, Colorado, on November 12, 1996, at 2:02p.m.

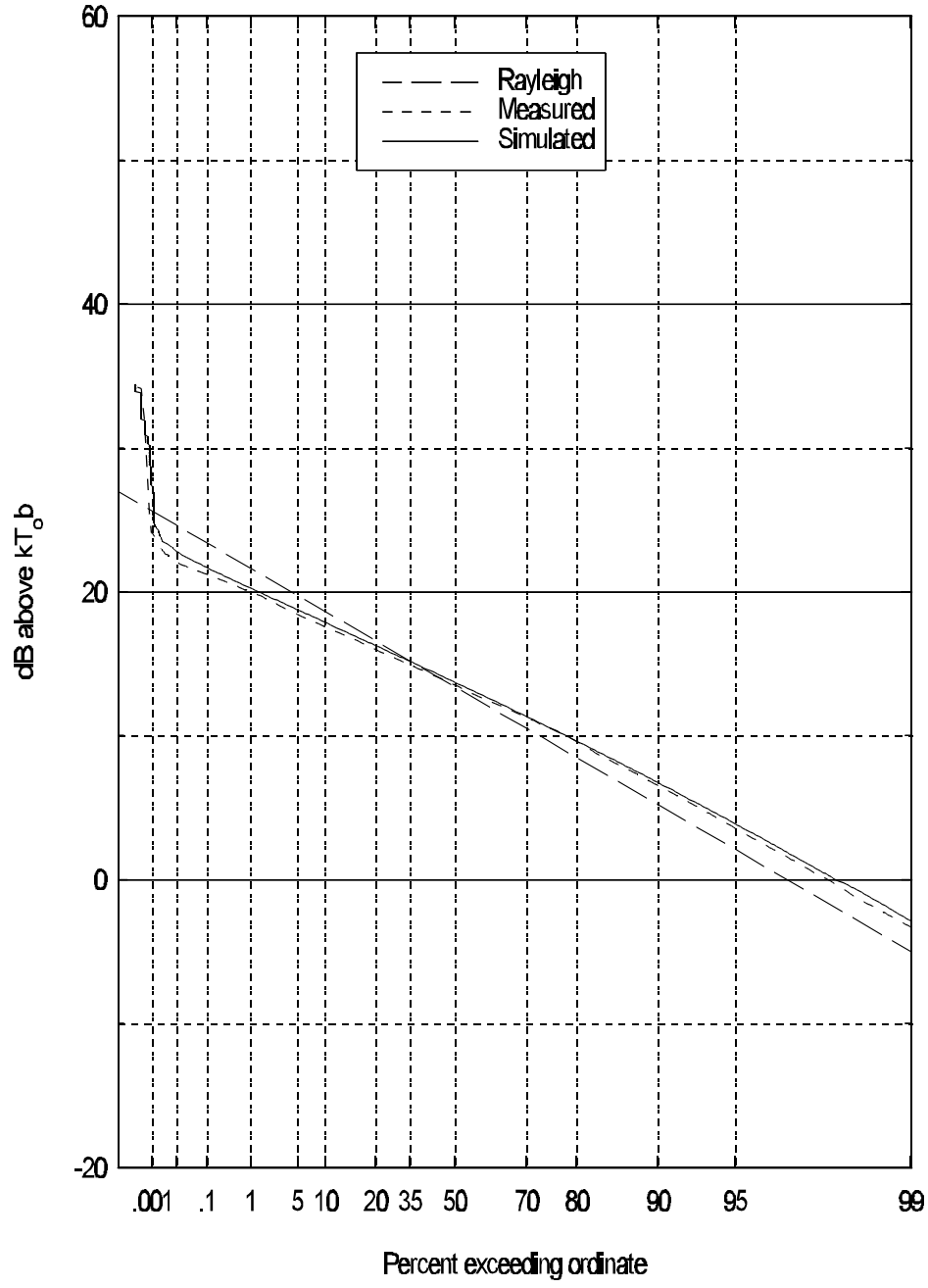

Figure 5.17 Class B noise from measurements in office park on November 27, 1996, from 12:20 to 12:50 a.m.

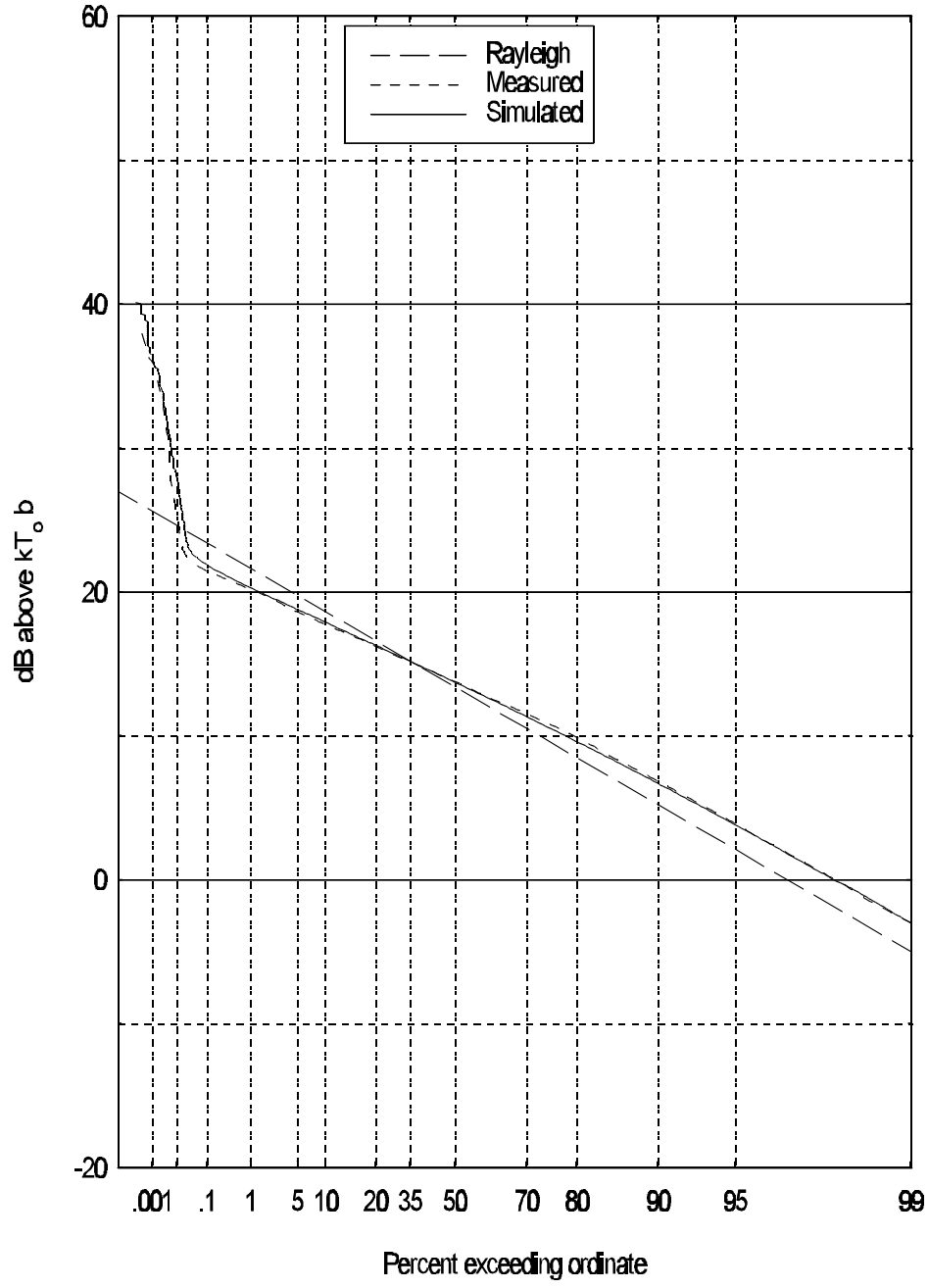

Figure 5.18 Class B noise from measurements in office park on November 27, 1996, from 11:15 to 11:45 a.m.

6. CONCLUSIONS

Spaulding hypothesized that man-made noise values, as reported in CCIR Report 258, may no longer be valid because of changes in electrical device technology such as the quieting of automotive ignition systems. These changes necessitate the measurement and modeling of man-made noise to determine if this is indeed the case. In this report the 136 to 138-MHz meteorological satellite band was measured and modelled, since space-to-earth links in this band are impacted greatly by man-made noise. We found that the characteristics of man-made noise in this band have changed, and we recommend further noise measurements in this band and others. The most striking results were the lack of within-the-hour variability of F_a in all environments, the drop in F_{am} for residential environments, and the relative quietness of the automobiles.

Graphs depicting the time-varying median, mean, and peak noise powers were presented in Section 3. The graphs show that within-the-hour variation of F_a is relatively small. CCIR Report 258 provided upper and lower decile values, D_u and D_l respectively, for within-the-hour variation of F_a as a function of frequency and environment. Spaulding and Stewart [14] have analyzed the data used to obtain D_u and D_l and have found it appropriate to use D_u = 9.7 dB and D_l = 7 dB, independent of environment or frequency. These decile values correspond to a within-the-hour standard deviation of approximately 6.6 dB. Clearly our measurements and those used for CCIR Report 258 differ significantly in within-the-hour variability.

The measured F_{am}, presented in Section 4, was 18.0, 6.0, and 6.3 dB for business, residential, and rural environments. CCIR Report 258 gives 17.6, 13.3, and 8.0 dB for the same environments [2]. Only residential F_{am} has changed appreciably from those values reported by the CCIR. These findings are significant for radio link designers. The discussion in Section 4 indicates that the CCIR noise measurement data were collected and analyzed somewhat differently. In particular, (1) the CCIR noise measurement data were collected during “mobile runs” through a “measurement area” while the measurements in this report were collected while stationary, (2) CCIR measurement data contained more location variability but not as much hour-to-hour time variability as the measurements in this report, and (3) CCIR estimates of F_{am} were dependent upon its behavior over 8 frequencies, whereas the estimate in this report is derived from measurements in a single frequency. Further measurements and analysis are needed to determine if these changes in measurement and analysis methods have impacted our conclusions.

Measurements of automobile noise suggest that automobiles are no longer a significant VHF noise source. In fact, stretches of urban highway were found to be quiet enough to coin the "light urban" environment classification. For example, Figure 3.6 shows automobile noise along an isolated mountain canyon road with an F_a of approximately 4 dB and Figure 3.3a shows automobile noise along an interstate highway adjacent to an office park with an F_a of approximately 7 dB. Spaulding's measurements [1] predict an F_a of approximately 15 dB for locations adjacent to interstate highways.

Power-line noise was noticed throughout the measurement campaign. Our limited measurements of power transmission- and distribution-lines indicate that this problem still exists. The power-line

measurements were conducted in a rural setting on a road perpendicular to a high-voltage transmission line and parallel to a lower voltage distribution line. Measurements near the high-voltage transmission line did not show an unusually high F_a at 136-138 MHz. Along the road, farther from the high-voltage transmission line, yet still near the lower voltage distribution line, the noise was found to be highly variable. This variability due to power lines is likely to be experienced in business, residential, and rural areas.

Computers were found to be capable of generating a significant amount of noise in this band. A simple experiment was conducted in a rural setting which documented the noise from two randomly selected computers. One of the computers was found to be noisy while the other was relatively quiet. Measurements outside our laboratory indicated that a telecommunication "switch" with an embedded computer introduced a narrowband continuous tone in the measurement receiver passband. Further study is needed to determine how narrowband noise power from computers and other electronic devices within a building would impact a receiving antenna mounted on or near an office building.

Analysis of noise APD's revealed a wide spectrum of noise types. Nakagami-Rice interference was found in several bussiness locations. This interference has a constant component along with a Gaussian component. Class A pulsed interference (emission bandwidth less than measurement bandwidth) was measured infrequently in all environments. Generally several hours passed between Class A interference events. We speculate that Class A noise events may be the result of line spectra generated from electrical devices.

Class B pulsed interference (emission bandwidth greater than measurement bandwidth) is by far the most common. Middleton spent considerable effort in modelling this class of noise. Using the ideas put forward by Middleton, we constructed a simplified noise model dependent upon a small set of parameters that were derived from the measurements. Using this approach we were able to simulate noise with first-order statistics that agreed with our measurements.

7. REFERENCES

[1] A.D. Spaulding and R.T. Disney, "Man-made radio noise, part 1:estimates for business, residential, and rural areas," Office of Telecommunications Report OT 74-38, Jun. 1974.

[2] CCIR, "Man-made radio noise," Report 258-5, International Radio Consultive Committee, International Telecommunications Union, Geneva, Switzerland, 1990.

[3] CCIR, "World distribution and characteristics of atmospheric radio noise," Report 322, International Radio Consultive Committee, International Telecommunications Union, Geneva, Switzerland, 1964.

[4] A.D. Spaulding, "The roadway natural and man-made noise environment," IVHS Journal, 2, pp. 175-211, 1995.

[5] A.D. Spaulding, "The natural and man-made noise environment in personal communications services bands," NTIA Report 96-330, May 1996.

[6] N.G. Riley and K. Docherty, "Modeling and measurement of man-made radio noise in the VHF-UHF Band," *Proc. Of the Ninth Internat. Conf. On Ant. Prop*., vol. 2. Pp. 313-316.

[7] S.N. Murthy and G. Krishnamraju, "interference to low earth orbit satellite (LEOS) services in VHF band from ground based emissions," IETE Technical Review, 12, pp. 325-329, 1995.

[8] G.H. Hagn, "Selected radio noise topics," SRI International Final Report, Project 45002, Contract No. NT83RA6-36001, 1984.

[9] W.M. Weiner, S.P. Cruze, C. Li, and W.J. Wilson, "*Monopole Elements on Circular Ground Planes*," Norwood, MA: Artech House, 1987.

[10] NOAA, "The Tiros-N/NOAA A-G Satellite Series," NOAA Technical Memorandum NESS 95, Aug. 1979.

[11] F.H. Sanders and V.S. Lawrence, "Broadband Spectrum Survey at Denver, Colorado," NTIA Report 95-321, Sept. 1995.

[12] V.L. Chartier, "The location, correction and prevention of RI and TVI sources from overhead power lines," IEEE 76-CH1163-5-PWR, pp. 12-19, 1976.

[13] P.L. Rice, A.G. Longley, K.A. Norton, and A.P. Barsis, "Phase interference fading and service probability," Annex V in vol.2 of *Transmission loss predictions for tropospheric communication circuits*, NBS Technical Note 101, 1966.

[14] A.D. Spaulding and F.G. Stewart, "An updated noise model for use in IONCAP," NTIA Report 87-212, Jan. 1987.

[15] Middleton, D. "Statistical-physical models of man-made and natural radio-noise environments–Part I: First-order probability models of the instantaneous amplitude," Office of Telecommunications Report OT 74-36, April 1975.

[16] Middleton, D. "Statistical-physical models of man-noise and natural radio-noise environment–Part II: First-order probability models of the envelope and phase," Office of Telecommunications Report OT 76-86, April 1976.

[17] Middleton, D. "Statistical-physical models of man-made and natural radio-noise environments–Part III: First-order probability models of the instantaneous amplitude of Class B interference," NTIA Contractor Report 78-1, June 1978.

[18] Middleton, D. "Statistical-physical models of man-made and natural radio-noise environments–Part IV: Determination of the first-order parameters of Class A and Class B interference, NTIA Contractor Report 78-2 Sept. 1978.

[19] G.H. Hagn, "Man-made radio noise and interference," in *Proc. Of AGARD Conf. No. 420,* Lisbon, Portugal, Oct. 26-30, 1987, pp. 5-1 to 5-15.

[20] M. Abramowitz and I.A. Stegun, *Handbook of Mathematical Functions*, NBS Applied Math Series 55, New York, NY: Dover Pub., 1964.

[21] W. Weibull, "A statistical distribution function of wide applicability," *J. Appl. Mech*., 18, pp. 293-297, 1951.

[22] M.C. Jeruchim, P. Balaban, and K.S. Shanmugan, *Simulation of communication Systems*, New York, NY: Plenum Press, 1992.

This Page Intentionally Left Blank

This Page Intentionally Left Blank

APPENDIX A: RECEIVER SPECIFICATIONS SUMMARY

This appendix summarizes the noise measurement receiver component and system specifications.

A.1 Receiver Description

Design: Single Conversion Superheterodyne
Detection: Log video
Radio frequency range: 136 - 138 MHz
Intermediate frequency: 10.7 MHz
Local oscillator range: 125.3- 127.3 MHz
Image frequency range: 114.6 to 116.6 MHz
Predetection 3-dB bandwidth: 32 kHz

A.2 Component Specifications

The acronyms in front of each component specification are used in Figure 2.2.

ANT, antenna: quarter-wave monopole mounted on center of van roof mounted ground plan 3.6 m long and 1.6 m wide
F1, bandpass filter: 3-pole Chebychev, 0.1-dB ripple, 4.1 MHz 3-dB bandwidth, 0.3-dB loss
A1, amplifier: 37-dB gain, 8-dBm 1-dB compression point, 1.1-dB NF
F2, bandpass filter: 5-pole Chebychev, 0.1-dB ripple, 4.1 MHz 3-dB bandwidth, 1.7-dB loss
M, mixer: 8-dB conversion loss, 14 dBm (input) 1-dB compression point
LO, Hewlet Packard HP8662 frequency synthesizer: +15 dBm output power
P1, attenuator: 10 dB
F3, low pass filter: 70 MHz 3-dB cutoff frequency, 0.0- dB loss
A2, amplifier: 22-dB gain, 9 dBm 1-dB compression point, 5.3 dB noise figure
P2, attenuator: 10 dB
F4, bandpass filter: 3-pole Chebychev, 0.1-dB ripple, 214 kHz 3-dB bandwidth, 9.5-dB loss
A3, amplifier: 28-dB gain, 18 dBm 1-dB compression point, 7-dB noise figure
P#, attenuator: 6 dB
A4, amplifier: 34-dB gain, 21 dBm 1-dB compression point, 5-dB noise figure
P4, attenuator: 10 dB
F5, bandpass filter:; 6-pole Chebychev, 1.0-dB ripple, 32 kHz 3-dB bandwidth, -1.8 dB loss
LA, log amplifier: 0.1 to 2.1 V, -80 to 0 dBm
ADC, digitizer: 0-10 V, 12 bit, 2.44 mV/ADC unit

A.3 System Specification

All system power specifications are the power at the receiver input.

Gain (measured from receiver input to log amplifier input): 63.0 dB
Noise figure: 2.9 dB
Predetection noise equivalent bandwidth: 34.2 kHz
Average noise power: 126 dBm in 34.2 kHz bandwidth, -171 dBm in 1 Hz bandwidth
1-dB compression point: -50 dBm
Two-tone test: 136.999 (f1) at -66 dBm combined with 137.001 (f2) at -66 dBm, -63 dBm combined input power, third order output (2f1-f2,2f2-f1): 136.997 and 137.003 are 42 dB down, fifth order output (3f1, 2f2, 3f2-2f1): 136.995 and 137.005 are 65 dB down
Log amplifier dynamic range (0.1 to 2.1 V): -143 dBm to -63 dBm in 3.2 kHz bandwidth, -188 dBm to -108 dBm in 1 Hz bandwidth
Image frequency rejection:> 100 dB